

# Accepted Manuscript

Synthesis, biological evaluation and molecular docking of benzimidazole grafted benz sulfamide -containing pyrazole ring derivatives as novel tubulin polymerization inhibitors

Yan-Ting Wang, Tian-Qi Shi, Hai-Liang Zhu, Chang-Hong Liu

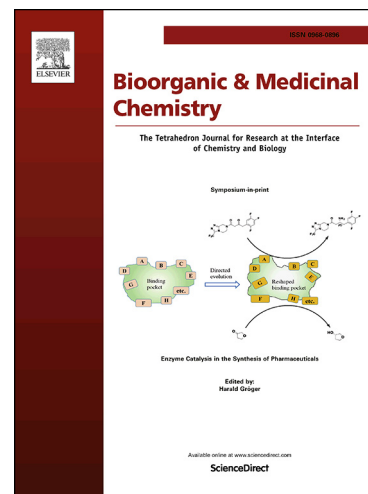
PII: S0968-0896(18)31676-6  
DOI: <https://doi.org/10.1016/j.bmc.2018.12.031>  
Reference: BMC 14680

To appear in: *Bioorganic & Medicinal Chemistry*

Received Date: 26 September 2018  
Revised Date: 14 December 2018  
Accepted Date: 21 December 2018

Please cite this article as: Wang, Y-T., Shi, T-Q., Zhu, H-L., Liu, C-H., Synthesis, biological evaluation and molecular docking of benzimidazole grafted benz sulfamide -containing pyrazole ring derivatives as novel tubulin polymerization inhibitors, *Bioorganic & Medicinal Chemistry* (2018), doi: <https://doi.org/10.1016/j.bmc.2018.12.031>

This is a PDF file of an unedited manuscript that has been accepted for publication. As a service to our customers we are providing this early version of the manuscript. The manuscript will undergo copyediting, typesetting, and review of the resulting proof before it is published in its final form. Please note that during the production process errors may be discovered which could affect the content, and all legal disclaimers that apply to the journal pertain.



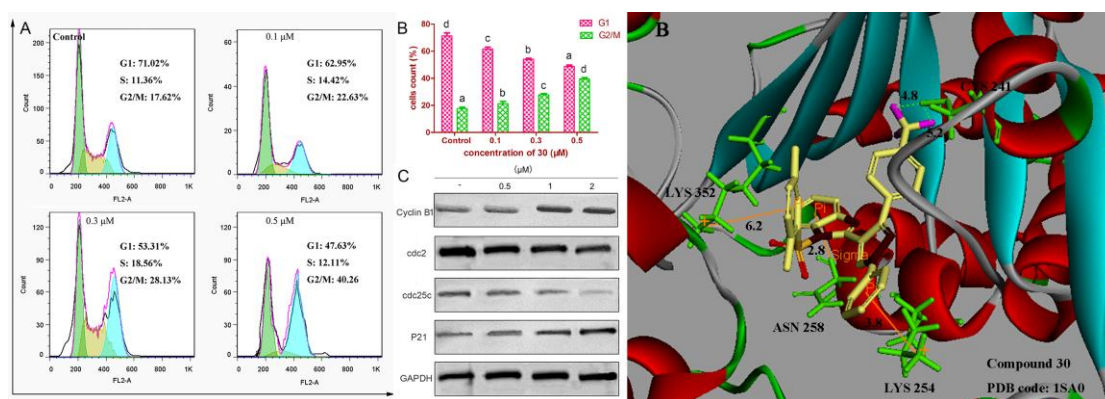
# Synthesis, biological evaluation and molecular docking of benzimidazole grafted benzulfamide -containing pyrazole ring derivatives as novel tubulin polymerization inhibitors

Yan-Ting Wang<sup>a,b,\*</sup>, Tian-Qi Shi<sup>a</sup>, Hai-Liang Zhu<sup>a,\*</sup>, Chang-Hong Liu<sup>a,\*</sup>

<sup>a</sup> State Key Laboratory of Pharmaceutical Biotechnology, Nanjing University, Nanjing 210093, P. R. China

<sup>b</sup> Department of Environmental Science & Engineering, Fudan University, Shanghai 200433, P. R. China

\*Corresponding authors. Tel. & fax: +86-25-89682572; e-mail: [zhuhl@nju.edu.cn](mailto:zhuhl@nju.edu.cn),  
[chliu@nju.edu.cn](mailto:chliu@nju.edu.cn)



Effect of compound **30** on cell cycle progression of A549 cells and G2/M-related proteins; 3D diagram of the interaction between compound **30** and the colchicine binding site.

A series of novel benzimidazole grafted benzulfamide -containing pyrazole ring derivatives were designed, synthesized and evaluated for the inhibitory activity against tubulin polymerization and cancer cells. Also the docking simulation of these compounds was conducted.

**Abstract:** Tubulin-targeting drugs have increasingly become the focus of anticancer drugs research. Twenty-five novel benzimidazole grafted benzulfamide -containing pyrazole ring derivatives were synthesized and evaluated for bioactivity as potential tubulin polymerization inhibitors. Among them, compound **30** showed the most excellent inhibition against tubulin assembly ( $IC_{50} = 1.52 \mu M$ ) and *in vitro* growth inhibitory activity against a panel of four human cancer cell lines ( $IC_{50} = 0.15, 0.21, 0.33$  and  $0.17 \mu M$ , respectively for A549, HeLa, HepG2 and MCF-7). It could also validly induce A549 cell apoptosis, cause cell cycle arrest in G2/M phase and disrupt the cellular microtubule network. These results, along with molecular docking data, provided an important basis for further optimization of compound **30** as a potential anticancer agent.

**Keywords:** benzimidazole; benzulfamide; pyrazole; tubulin; inhibition; apoptosis; molecular docking

## 1. Introduction

Microtubules are polar cytoskeletons, which are assembled by the aggregation of  $\alpha$ - and  $\beta$ - tubulin heterodimers in a head-to-tail manner to form hollow cylindrical filaments. [1] They are structural components of the mitotic spindle, and dynamic microtubules play an important role in several cellular processes including intracellular trafficking, cell migration, cell skeleton development and cell division. [2] These functions are probably correlated with post-translational modifications such as acetylation, polyglycylation, polyglutamylolation, and tyrosination of tubulin. [3] In the M-phase of cell cycle, microtubules assembled as a spindle direct the chromosomes into individual cells; they therefore are crucial targets for the development of anticancer agents. Compounds that interfere with the microtubulin equilibria in cells are very effective in the treatment of human cancer [4, 5]. They interfere with this dynamic equilibrium by binding to tubulins and induce cell cycle arrest, resulting in cell death [6, 7].

Natural products such as paclitaxel, vinca alkaloids, and colchicine **a** (**Fig. 1**) were found to bind to microtubules at specific binding sites and thus display remarkable microtubule-targeting activity. These microtubule-targeting compounds are functionally categorized into microtubule-stabilizers and microtubule-destabilizers [8]. The taxanes such as paclitaxel and docetaxel stabilize microtubules by preventing depolymerization of tubulin. The vinca alkaloids (eg., vincristine, vinblastine, and vinorelbine) and colchicine inhibit the polymerization of tubulin [6, 9]. Disruption of tubulin dynamics leads to cell cycle arrest in the G2/M phase and induction of apoptosis [10, 11].

Many molecular modeling studies and experimental data have demonstrated how these inhibitors bind to the active site of tubulin. [12-15]. Colchicine binding is considered a universal property of higher eukaryotic tubulin [16]. Compounds that bind to the colchicine site have been the subject of researchers' efforts to find new agents that can address the limitations of existing tubulin-targeted drugs. [17, 18] Combretastatin A-4 (CA-4) **b** (**Fig. 1**) is the most active member of the combretastatin family, isolated from the African tree *Combretum caffrum*. CA-4 exhibits strong

antitubulin activity by binding to the colchicine-site and underwent phase II and phase III studies in clinical. [19]

Over the past decade, a growing number of synthetic compounds related to benzenesulfonamide have been reported to inhibit tubulin polymerization, such as ABT-751 (**Fig. 1**) [20], indisulam (**Fig. 1**), HMN-214 (**Fig. 1**) [21] and 1-phenylsulfonyl-2-(1-methylindol-3-yl)-benzimidazole **f** (**Fig. 1**) [22]. Mei-Jung Lai's earlier work on the modification of ABT-751 revealed that the benzenesulfonamide moiety is crucial for the compound's anticancer activity. [22-24] In addition, biaryl moieties have been frequently observed in the development of antitubulin agents. [25, 26] Compound **g** (**Fig. 1**), with both benzenesulfonamide and biaryl moieties, was found in previous study to have remarkable antiproliferative activity. [24] Literature surveys indicated that the *N*-sulfonyl-aminobiaryl moiety has been comprehensively included in various heterocycles such as carbazole, [27] phenanthridinones, and phenanthridines, benzimidazole. [28, 29]

In order to search for novel antitubulin agents, we designed a class of *N*-sulfonyl-aminobiaryl moiety analogs based on benzimidazole grafted pyrazole scaffold. We chose benzimidazole and pyrazole moieties because they showed widely biological activities. Benzimidazole is a heterocyclic compound known for its antibacterial, antifungal, antiparasitic, anti-inflammatory and antiviral activities. [30] Some studies have also shown that benzimidazole-containing drugs have good antitumor activity [31-35], such as Nocodazole **h** and compound **i** (**Fig. 1**). In addition, pyrazoline derivatives have been reported to possess anticancer, antimicrobial and anti-inflammatory activities. [36-39], such as compound **j** (**Fig. 1**).

To our knowledge, no reports have been dedicated to the synthesis of benzimidazole grafted benzsulfamide -containing pyrazole ring derivatives. This combination was suggested in an attempt to investigate the inhibitory activity against tubulin. Through a combined virtual and experimental screening approach, we identified several compounds as potent tubulin inhibitors, especially compound **30**.

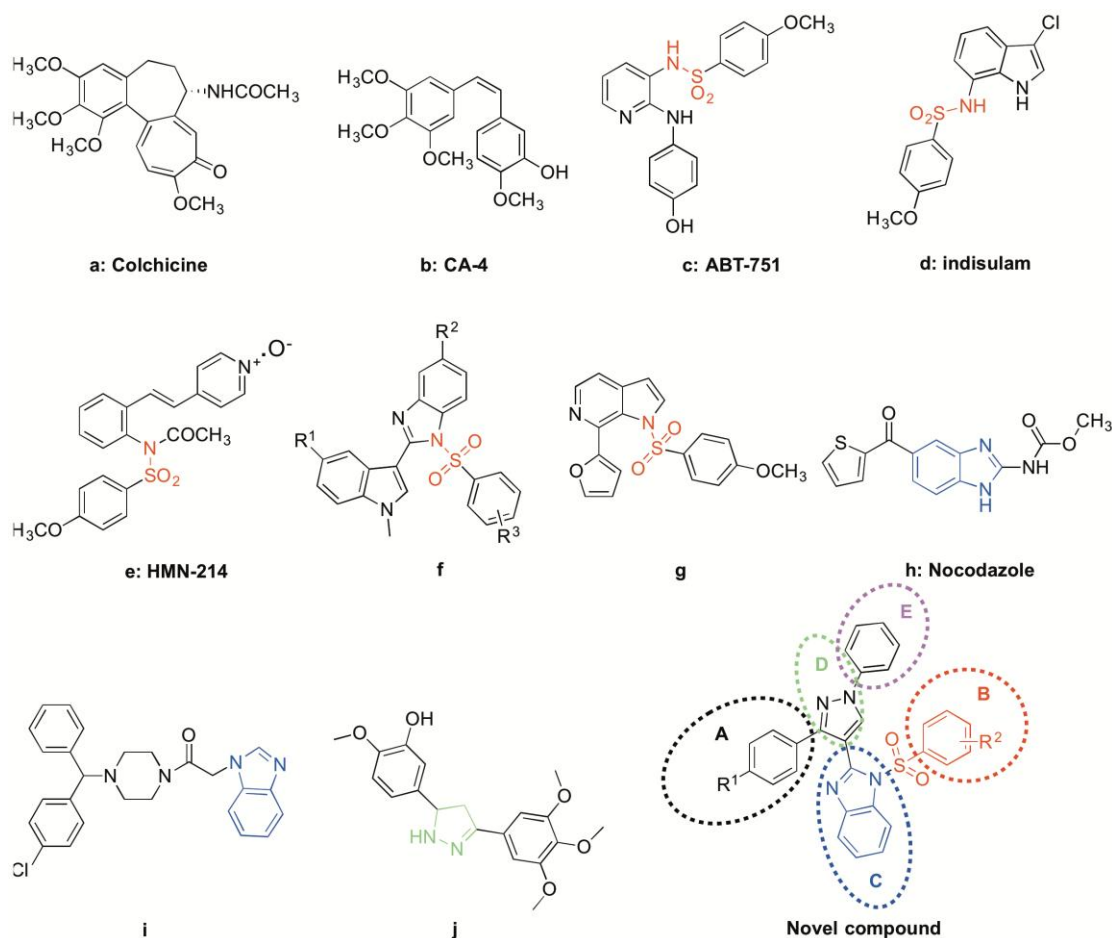
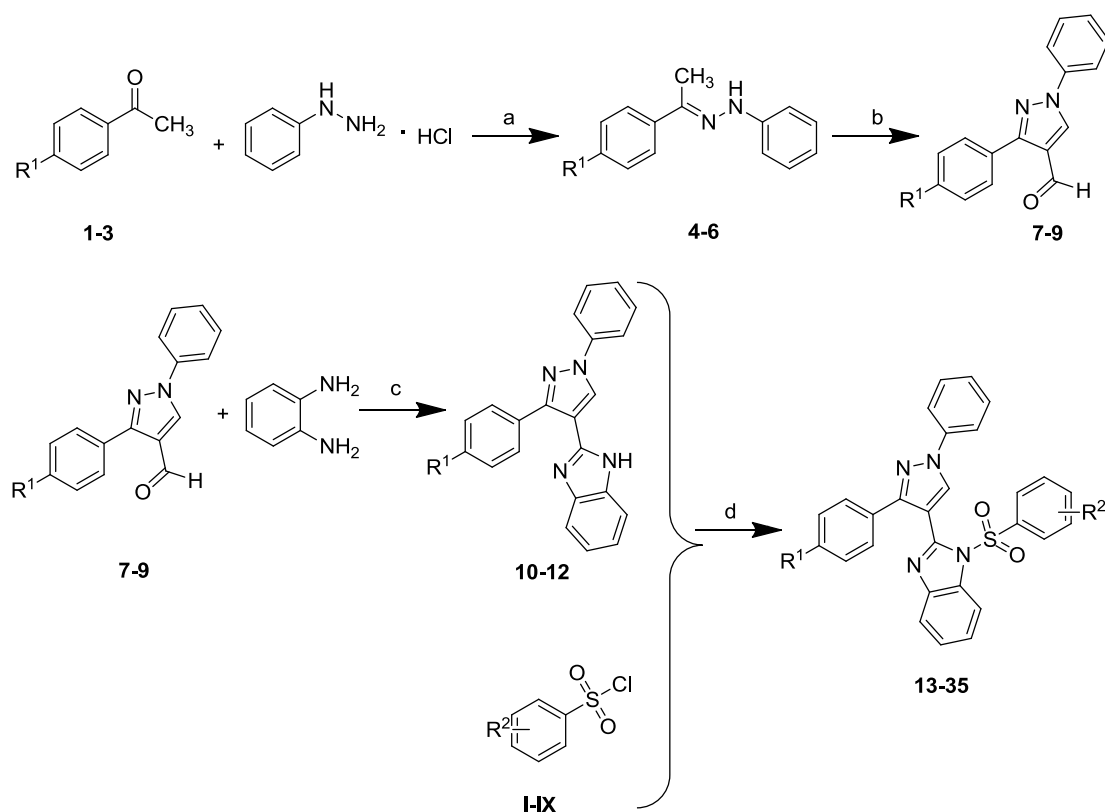


**Fig. 1.** Potential inhibitors and new inhibitor of tubulin polymerization.

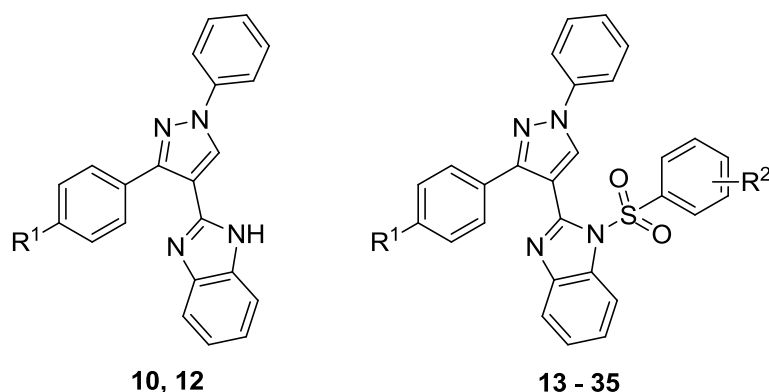
## 2. Results

### 2.1. Chemistry

The synthesis of compounds **10**, **12-35** followed the general pathway was outlined in **Scheme 1**. The target compounds were obtained in four steps as described in experimental section. All of the synthetic compounds are being reported for the first time (**Table 1**) and gave satisfactory analysis and spectroscopic data. <sup>1</sup>H NMR, <sup>13</sup>C NMR, melting test, mass spectroscopy and elemental analysis, and analysis results were in full accordance with their depicted structures.



**Scheme 1.** General synthesis of novel compounds (**10**, **12-35**). **I**: benzene sulfonyl chloride; **II**: *p*-toluenesulfonyl chloride; **III**: 4-methoxy benzene sulfonyl chloride; **IV**: 2,5-dimethoxy sulfonyl chloride; **V**: 4-nitrobenzenesulfonyl chloride; **VI**: 4-fluorobenzenesulfonyl; **VII**: 4-chlorobenzene sulfonyl chloride; **VIII**: 4-bromobenzene sulfonyl chloride; **IX**: 4-trifluoromethyl sulfonyl chloride; **1**, **4**, **7**, **10**:  $\text{R}_1 = \text{CH}_3$ ; **2**, **5**, **8**, **11**:  $\text{R}_1 = \text{F}$ ; **3**, **6**, **9**, **12**:  $\text{R}_1 = \text{CF}_3$ ; **13-35**: (Table 1). Reagents and conditions: (a)  $\text{CH}_3\text{CH}_2\text{ONa}$ ,  $\text{H}_2\text{O}$ , rt, 4 h; (b) DMF,  $\text{POCl}_3$ ,  $0^\circ\text{C}$ , 15min, rt, 3 h; (c) Sodium metabisulfite, DMF,  $110^\circ\text{C}$ , 4 h; (d) EDC·HCl, triethylamine,  $\text{CH}_2\text{Cl}_2$ , room temperature, 12 h.

**Table 1.** Structures of compounds **10**, **12-35**

Compounds	R <sup>1</sup>	R <sup>2</sup>	Compounds	R <sup>1</sup>	R <sup>2</sup>
<b>10</b>	-CH <sub>3</sub>	–	<b>24</b>	-F	4-F
<b>12</b>	-CF <sub>3</sub>	–	<b>25</b>	-F	4-Cl
<b>13</b>	-CH <sub>3</sub>	H	<b>26</b>	-F	4- Br
<b>14</b>	-CH <sub>3</sub>	4-CH <sub>3</sub>	<b>27</b>	-F	4-CF <sub>3</sub>
<b>15</b>	-CH <sub>3</sub>	2,5-(CH <sub>3</sub> ) <sub>2</sub>	<b>28</b>	-CF <sub>3</sub>	H
<b>16</b>	-CH <sub>3</sub>	4-F	<b>29</b>	-CF <sub>3</sub>	4-OCH <sub>3</sub>
<b>17</b>	-CH <sub>3</sub>	4-Cl	<b>30</b>	-CF <sub>3</sub>	2,5-(CH <sub>3</sub> ) <sub>2</sub>
<b>18</b>	-CH <sub>3</sub>	4-Br	<b>31</b>	-CF <sub>3</sub>	4-NO <sub>2</sub>
<b>19</b>	-CH <sub>3</sub>	4-CF <sub>3</sub>	<b>32</b>	-CF <sub>3</sub>	4-F
<b>20</b>	-F	H	<b>33</b>	-CF <sub>3</sub>	4-Cl
<b>21</b>	-F	4-OCH <sub>3</sub>	<b>34</b>	-CF <sub>3</sub>	4-Br
<b>22</b>	-F	2,5-(CH <sub>3</sub> ) <sub>2</sub>	<b>35</b>	-CF <sub>3</sub>	4-CF <sub>3</sub>
<b>23</b>	-F	4-NO <sub>2</sub>			

## 2.2. Crystal structure determination

The crystal structures of compounds **20** and **24** were determined by X-ray diffraction analysis. The crystal data presented in **Table 2** and **Fig. 2** gave the perspective views of **20** and **24** with the atomic labeling system. The crystallographic data have been deposited at the Cambridge Crystallographic Data Centre (CCDC) and the deposition numbers of **20** and **24** are 1514296 and 1514297, respectively.

**Table 2.** Crystallographic and Experimental Data for compounds **20** and **24**

Compounds	<b>20</b>	<b>24</b>
Formula	C <sub>28</sub> H <sub>19</sub> FN <sub>4</sub> O <sub>2</sub> S	C <sub>30</sub> H <sub>24</sub> F <sub>2</sub> N <sub>4</sub> O <sub>3</sub> S
Formula weight	494.53	558.59
Crystal system	Monoclinic	Monoclinic
Space group	<i>C2/c</i>	<i>P-1</i>
<i>a</i> (Å)	29.137(9)	8.2599(3)
<i>b</i> (Å)	8.721(3)	9.0030(3)
<i>c</i> (Å)	21.941(7)	19.0369(6)
$\alpha$ (°)	90.00	77.3790(10)
$\beta$ (°)	113.919(8)	79.4050(10)
$\gamma$ (°)	90.00	82.735(2)
<i>V</i> (Å <sup>3</sup> )	5097(3)	1352.39(8)
<i>Z</i>	8	2
<i>D<sub>c</sub></i> (g•cm <sup>-3</sup> )	1.289	1.372
$\mu$ (mm <sup>-1</sup> )	0.166	0.173
<i>F</i> (000)	2048	580
$\theta$ rang(°)	2.03-28.82	2.22-28.30
Reflns collected	69038	29434
Reflns unique	6485	6551
Goodness-of-fit on <i>F</i> <sup>2</sup>	1.080	1.000
<i>RI</i> , <i>wR</i> <sub>2</sub> [ <i>I</i> > 2σ( <i>I</i> )]	0.2394, 0.5698	0.1356, 0.3521
<i>RI</i> , <i>wR</i> <sub>2</sub> [all data]	0.2937, 0.6669	0.1700, 0.4243
Max, minΔρ(e Å <sup>-3</sup> )	1.320, -1.093	1.202, -0.517

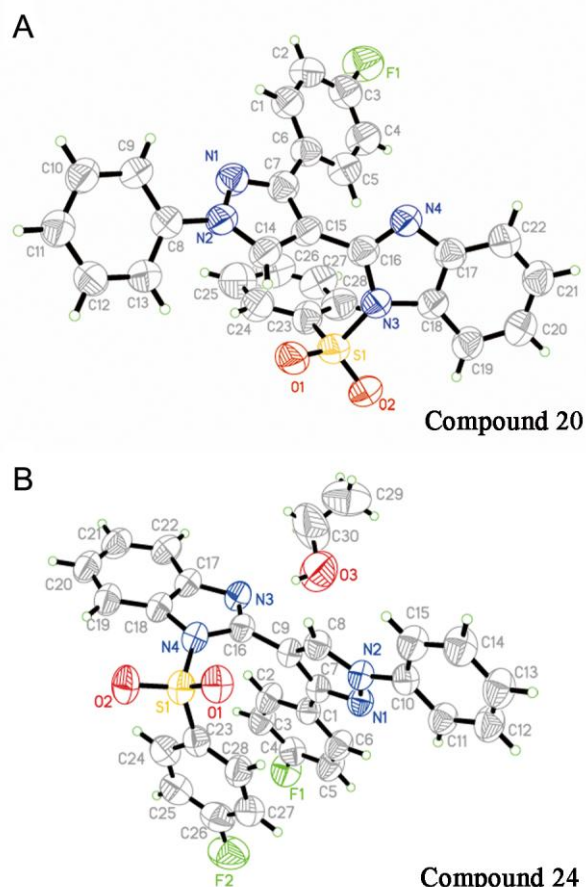


**Fig. 2.** (A) Crystal structure diagram of compound **20**. (B) Crystal structure diagram of compound **24**. H atoms are shown as small spheres of arbitrary radii.

### 2.3. Biological evaluation

#### 2.3.1. *In vitro* antiproliferative activities (cell viability was assessed by MTT assay [40])

All novel derivatives **10**, **12-35** were evaluated for their inhibitory effect on growth of four cancer cell lines [human lung adenocarcinoma epithelial cell line (A549), carcinoma of cervix cell line (Hela), human hepatoma cell line (HepG2) and human breast cancer cell (MCF-7)] with positive contrast drugs colchicine and CA-4. Cells were treated with different concentrations of the given compounds, and the viabilities were measured by MTT assay. Results (depicted in **Table 3**) showed that most of the target compounds can effectively inhibit the proliferation of the four tumor cells, especially for A549 cells. Compounds **22**, **29**, **30** showed better antiproliferative activities than colchicine ( $IC_{50} = 0.22 \mu\text{M}$  for A549,  $IC_{50} = 0.36 \mu\text{M}$

for HeLa,  $IC_{50} = 0.42 \mu\text{M}$  for HepG2,  $IC_{50} = 0.44 \mu\text{M}$  for MCF-7), and compound **30** is better than CA-4 ( $IC_{50} = 0.16 \mu\text{M}$  for A549,  $IC_{50} = 0.24 \mu\text{M}$  for HeLa,  $IC_{50} = 0.33 \mu\text{M}$  for HepG2,  $IC_{50} = 0.18 \mu\text{M}$  for MCF-7). The  $IC_{50}$  values of these compounds against the four cell lines were between 0.15 and 7.26  $\mu\text{M}$ .

According to the data in **Table 3**, we predicted that the difference of biological activities among the tested compounds might be correlated to the variation and modifications of the structure. For example, compounds **10** and **12** showed lower bioactivities than any other novel compounds, which demonstrated that benzenesulfonyl was an important structure contributing to the bioactivities of these compounds.

Moreover, various substituents of  $R^1$  in the *para*-position of A-ring led to different bioactivities, if the substituents of B-ring kept immutability. Basically, the bioactivities of the compounds were increased in the following order:  $\text{CF}_3 > \text{F} > \text{CH}_3$ , which could be observed from the comparison:  $30 > 22 > 15$ ,  $29 > 21$ ,  $28 > 20 > 13$ ,  $31 > 23$ ,  $35 > 27 > 19$ ,  $34 > 26 > 18$ ,  $33 > 25 > 17$ ,  $12 > 10$ .

Compounds with different groups in the B ring were compared in a similar way, which showed electron-donating groups (such as  $\text{OCH}_3$ ,  $\text{CH}_3$ ) in the B ring were preferable to electron-withdrawing groups (such as  $\text{NO}_2$ , F). For instance, the active gradients for compounds were  $29 > 28 > 31 > 35 > 34 > 32 > 33$ ,  $22 > 21 > 20 > 23 > 27 > 26 > 24 > 25$ ,  $15 > 14 > 13 > 19 > 18 > 16 > 17$ . In addition, the more electron-donating substituted groups in the B-ring, the better the antiproliferative activity it was, and this could be demonstrated from the comparison:  $15 > 14$ .

From the analysis mentioned above, some structure-activity relationship (SAR) could be concluded: the presence of benzenesulfonyl was crucial in the cancer cell inhibition; compounds with trifluoromethyl substituted *para*-position of A-ring and methoxy and methyl substituted B-ring were found to be the most favorable for the anticancer activity. Based on structure, activity, and structure-activity analysis, we can conclude that compound **30** is the most bioactive compound against proliferation of cancer cell lines A549, HeLa, HepG2 and MCF-7 with  $IC_{50}$  values of 0.15, 0.21, 0.33 and 0.17  $\mu\text{M}$ , respectively.

**Table 3.** *In vitro* Inhibition of Tubulin Polymerization and growth inhibition of A549, HeLa, HepG2 and MCF-7 cells by compounds **10**, **12-35**, combretastatin A-4 and colchicine.

Compounds	IC <sub>50</sub> <sup>a</sup> ± SD <sup>b</sup> ( $\mu$ M)					Colchicine binding	Vinblastine binding
	A549	HeLa	HepG2	MCF-7	Tubulin <sup>c</sup>	inhibition <sup>d</sup> % ± SD	inhibition <sup>e</sup> % ± SD
<b>10</b>	4.01 ± 0.43	4.95 ± 0.04	6.26 ± 0.08	7.26 ± 0.47	45.73 ± 1.21	40 ± 1.4	0.05 ± 1.5
<b>12</b>	3.62 ± 0.21	4.67 ± 0.32	6.03 ± 0.23	6.33 ± 0.38	44.66 ± 0.49	44 ± 2.9	-0.03 ± 2.1
<b>13</b>	0.76 ± 0.20	0.82 ± 0.09	0.96 ± 0.31	0.83 ± 0.62	3.84 ± 0.74	74 ± 0.9	0.21 ± 1.4
<b>14</b>	0.46 ± 0.35	0.48 ± 0.21	0.52 ± 0.02	0.57 ± 0.29	2.64 ± 0.81	66 ± 0.2	0.18 ± 2.8
<b>15</b>	0.27 ± 0.36	0.37 ± 0.05	0.46 ± 1.03	0.51 ± 0.74	1.97 ± 0.33	82 ± 1.6	0.07 ± 1.5
<b>16</b>	3.24 ± 0.43	3.67 ± 0.17	5.06 ± 0.35	5.27 ± 0.65	29.13 ± 0.16	53 ± 0.1	0.07 ± 0.3
<b>17</b>	3.55 ± 0.52	4.06 ± 1.04	5.52 ± 0.16	5.93 ± 0.86	32.04 ± 0.28	38 ± 0.7	0.24 ± 0.4
<b>18</b>	1.86 ± 0.27	2.34 ± 0.06	3.04 ± 0.27	3.16 ± 0.09	17.69 ± 0.05	48 ± 0.9	-0.38 ± 1.4
<b>19</b>	1.46 ± 0.02	1.52 ± 0.12	1.93 ± 0.09	2.34 ± 1.07	11.32 ± 0.19	55 ± 0.1	0.21 ± 2.6
<b>20</b>	0.55 ± 0.16	0.68 ± 0.42	0.72 ± 1.24	0.69 ± 0.48	3.49 ± 0.21	62 ± 1.6	0.05 ± 1.4
<b>21</b>	0.35 ± 0.04	0.39 ± 0.37	0.47 ± 0.63	0.53 ± 0.62	2.31 ± 0.44	77 ± 0.8	2.98 ± 1.2
<b>22</b>	0.20 ± 0.14	0.32 ± 0.08	0.41 ± 0.45	0.43 ± 0.73	1.82 ± 1.32	88 ± 0.4	0.62 ± 0.8
<b>23</b>	1.03 ± 0.35	1.17 ± 0.29	1.34 ± 0.05	1.37 ± 0.46	7.27 ± 0.79	51 ± 4.2	-0.04 ± 0.3
<b>24</b>	2.37 ± 0.07	2.44 ± 0.02	3.52 ± 1.07	3.67 ± 1.24	20.33 ± 1.28	48 ± 0.5	1.32 ± 1.1
<b>25</b>	3.17 ± 0.25	3.45 ± 0.14	4.23 ± 0.38	4.96 ± 1.08	25.67 ± 0.56	48 ± 0.4	-2.09 ± 2.7
<b>26</b>	1.72 ± 0.31	2.04 ± 0.29	2.55 ± 0.25	2.63 ± 1.46	14.08 ± 1.33	51 ± 1.3	3.02 ± 2.2
<b>27</b>	1.28 ± 0.42	1.43 ± 0.33	1.68 ± 0.81	1.58 ± 0.49	8.06 ± 0.05	50 ± 0.7	0.51 ± 2.7
<b>28</b>	0.48 ± 0.06	0.56 ± 0.46	0.59 ± 0.15	0.63 ± 0.72	2.96 ± 0.39	61 ± 2.4	0.52 ± 3.6
<b>29</b>	0.17 ± 0.51	0.25 ± 1.22	0.37 ± 0.72	0.42 ± 0.06	1.63 ± 0.06	85 ± 1.3	0.03 ± 2.3
<b>30</b>	0.15 ± 0.05	0.21 ± 0.67	0.33 ± 0.06	0.17 ± 0.23	1.52 ± 1.07	91 ± 4.1	0.06 ± 1.7
<b>31</b>	0.79 ± 0.01	0.95 ± 2.01	1.07 ± 0.90	1.13 ± 0.17	4.56 ± 0.73	63 ± 0.6	0.14 ± 4.2
<b>32</b>	1.74 ± 0.71	2.19 ± 0.35	2.73 ± 1.24	3.12 ± 0.04	16.73 ± 0.58	54 ± 0.6	0.65 ± 4.4
<b>33</b>	2.56 ± 0.06	3.06 ± 0.48	3.93 ± 0.28	4.32 ± 0.23	21.36 ± 1.05	40 ± 0.6	0.73 ± 1.7
<b>34</b>	1.69 ± 0.27	1.86 ± 0.22	2.16 ± 0.56	2.47 ± 0.26	12.67 ± 1.32	52 ± 0.3	-0.07 ± 2.1
<b>35</b>	0.86 ± 0.04	0.97 ± 0.07	1.12 ± 0.73	1.24 ± 0.18	5.78 ± 0.66	54 ± 3.3	0.05 ± 2.4
Colchicine <sup>f</sup>	0.22 ± 0.12	0.36 ± 0.07	0.42 ± 0.12	0.44 ± 0.18	2.26 ± 0.25	—	—
CA-4 <sup>f</sup>	0.16 ± 0.04	0.24 ± 0.08	0.33 ± 0.12	0.18 ± 0.17	1.61 ± 0.31	89 ± 1.4	—

All experiments were independently performed at least three times.

<sup>a</sup>IC<sub>50</sub> values, which include those of the parent compounds colchicine and CA-4, are expressed as the compound concentration ( $\mu\text{mol/L}$  or  $\mu\text{M}$ ) that causes 50% inhibition of cell growth. The values are the average ( $\pm\text{SD}$ ) of three different measurements performed as described in the Experimental Section.

<sup>b</sup>SD: standard deviation.

<sup>c</sup>Inhibition of tubulin polymerization.

<sup>d</sup>Inhibition of [<sup>3</sup>H]colchicine binding.

<sup>e</sup>Inhibition of vinblastine binding.

<sup>f</sup>Used as positive controls.

### 2.3.2. Tubulin polymerization inhibition assay [41]

To investigate whether the antiproliferative activities of compounds **10**, **12-35** derived from an interaction with tubulin or not, these agents were evaluated for their inhibition of tubulin polymerization.

Before the inhibition assay, tubulin was extracted from pig brain and the purified protein was identified using SDS-PAGE gel electrophoresis (**Fig. 3A**). Tubulin inhibition results (**Table 3**) showed that these compounds exhibited different inhibitory activities against tubulin polymerization with IC<sub>50</sub> values ranging from 1.52 to 45.73  $\mu\text{M}$ . Compound **30** showed similar or even better inhibitory activities than the positive control agent CA-4 (IC<sub>50</sub> = 1.61  $\mu\text{M}$ ) on tubulin polymerization. While compounds **15**, **22**, **29** and **30** were better than colchicine (IC<sub>50</sub> = 2.26  $\mu\text{M}$ ). Compound **30** was the most potent compound as a tubulin polymerization inhibitor with an IC<sub>50</sub> of 1.52  $\mu\text{M}$ , which was similar to that of antiproliferative activities against the cancer cell lines. Moreover, most of the bioactive compounds showed not only tubulin polymerization inhibition, but also growth inhibition, which indicated the two bioactivities might be positively correlated.

To test the inhibitory effect of compound **30** on microtubule assembly *in vitro*, depolymerization activity was measured by the method described by Bonne *et al.* with some modification. [42] In the control samples, which were not treated with drugs, the

fluorescence intensity at 350 nm increased with time. Treating with colchicine, CA-4 or compound **30** resulted in various degrees of tubulin depolymerization (**Fig. 3B**). Compared to the control, compound **30** appeared to be slightly inhibiting tubulin polymerization at 1.0  $\mu\text{M}$ . However, when concentration of compound **30** was increased to 5.0  $\mu\text{M}$ , tubulin polymerization was nearly completely blocked just as 8.0  $\mu\text{M}$  CA-4 did, suggesting that tubulin polymerization was inhibited by compound **30** in a concentration-dependent manner. The inhibitory mechanism of compound **30** on microtubule morphology was similar to that of CA-4.

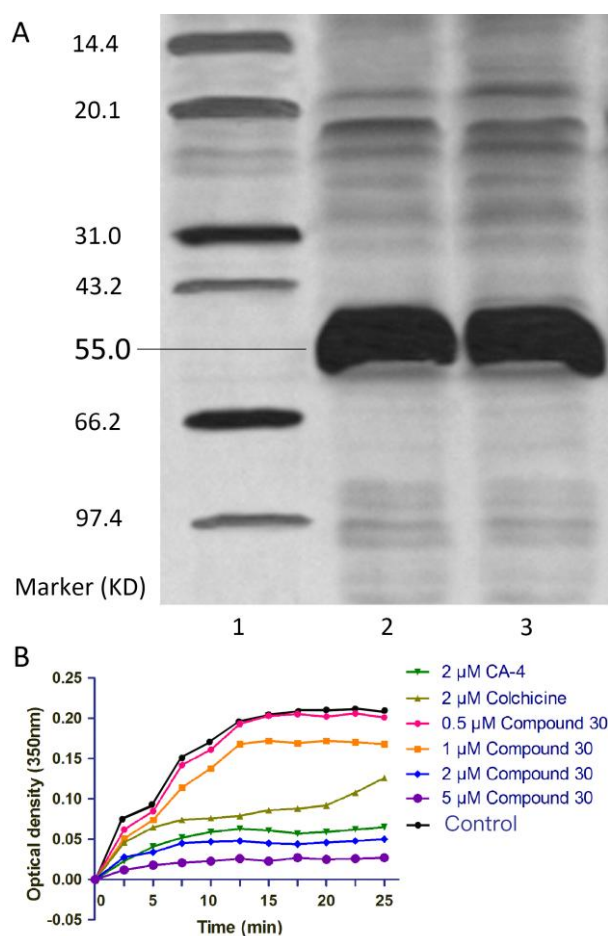


**Fig. 3.** (A) SDS-PAGE gel electrophoresis of purified tubulin extracted from pig brain. 1: Marker, 2 and 3: purified tubulin; (B) Effects assay of compound **30** on microtubule morphology. The evaluation of tubulin polymerization is in the presence of compound **30**, colchicine and CA-4 at 37 °C.

In addition, the new benzimidazole grafted benzulfamide -containing pyrazole ring derivatives were examined for potential inhibition of the binding of [<sup>3</sup>H]Colchicine to tubulin in parallel with CA-4 (**Table 3**). All except **10**, **12**, **17** and **33** were strong inhibitors of the binding reaction (48 - 91% inhibition ratio). What's more, compound **30** were stronger than CA-4 (89% inhibition ratio). In this assay, it was observed that compound **30** was the strongest inhibitor, which also proved that these compounds target tubulin at colchicine domain target. Furthermore, the synthesized compounds were also detected the binding site-specific competition with another type of tubulin polymerization inhibitor vinblastine, finally no compounds exerted significant competitive binding inhibition for vinblastine (**Table 3**). These outcomes validly illustrated that the binding site of the new compounds was colchicine binding site, not vinblastine binding site.

### 2.3.3. Cytotoxicity test

All the target compounds were evaluated for their toxicity against human kidney epithelial cell 293T and mouse primary hepatocytes with the median cytotoxic concentration (CC<sub>50</sub>) data of tested compounds by the MTT assay. As shown in **Table 4**, the minimum CC<sub>50</sub> of the 25 test compounds against 293T cells and mouse primary hepatocytes were 37.26  $\mu$ M and 55.33  $\mu$ M respectively, which indicated that these compounds were free cytotoxic activities *in vitro* to the given cells.

**Table 4.** The median cytotoxic concentration (CC<sub>50</sub>) data of all compounds against 293T cell and mouse primary hepatocytes

Compounds	CC <sub>50</sub> <sup>a</sup> ( $\mu$ M)		Compounds	CC <sub>50</sub> <sup>a</sup> ( $\mu$ M)	
	293T	Primary hepatocytes		293T	Primary hepatocytes
<b>10</b>	187.33	>300	<b>25</b>	93.12	231.28
<b>12</b>	166.74	158.66	<b>26</b>	238.93	>300
<b>13</b>	137.87	188.79	<b>27</b>	241.32	55.33
<b>14</b>	79.34	102.44	<b>28</b>	128.38	186.34
<b>15</b>	82.18	231.34	<b>29</b>	>300	87.36

<b>16</b>	128.32	167.45	<b>30</b>	223.10	132.48
<b>17</b>	167.43	215.63	<b>31</b>	163.21	178.43
<b>18</b>	158.66	>300	<b>32</b>	156.53	83.28
<b>19</b>	182.19	89.32	<b>33</b>	75.32	173.24
<b>20</b>	96.32	231.16	<b>34</b>	184.56	167.49
<b>21</b>	37.26	105.34	<b>35</b>	63.23	137.34
<b>22</b>	54.20	121.67	<b>Colchicine</b>	129.32	152.78
<b>23</b>	189.32	>300	<b>CA-4</b>	162.35	178.32
<b>24</b>	218.32	174.37			

<sup>a</sup>The cytotoxicity of each compound was expressed as the concentration of compound that reduced cell viability to 50% (CC<sub>50</sub>).

#### 2.3.4. Analysis of apoptosis by fluorescence-activated cell sorting [43, 44]

Based on the antiproliferative and antitubulin activities, compound **30** with the most potent activity was chosen for deeper mechanism researches. In the apoptosis experiment, A549 cells treated with different concentrations of compound **30** were stained with annexin V-FITC/PI, and analyzed by flow cytometry. As depicted in **Fig. 4**, it was clear that annexin-V was accumulated in the A549 cells after treated with compound **30** at any given concentrations. Increase of the concentration of compound **30** could enhance the cell apoptosis by the ratio up to 7.98%, 12.64% and 18.84% at 0.1, 0.3 and 0.5  $\mu$ M respectively.

In addition, Apoptosis-related proteins were analyzed by western blot. These proteins were Bax, PARP, Bcl-2 and Caspase 3. As shown in **Fig. 4C**, the level of Bax was efficiently up-regulated and the level of anti-apoptotic proteins Bcl-2 was down-regulated. Caspases, which act as the central executioners of apoptosis, and their activation are mediated by various inducers. Synthesized as proenzymes, caspases are themselves activated by specific proteolytic cleavage reactions. Caspase-2, -8, -9, and -10 are termed apical caspases, which are usually the first to be activated in the apoptotic process. Following their activation, they in turn activate effector caspases, in particular caspase-3. Following treatment of A549 cells with compound **30** for 24 h

resulted in an up regulation of cleaved caspase-3 and PARP, which may be partially responsible for the apoptotic tendency of the A549 cells.

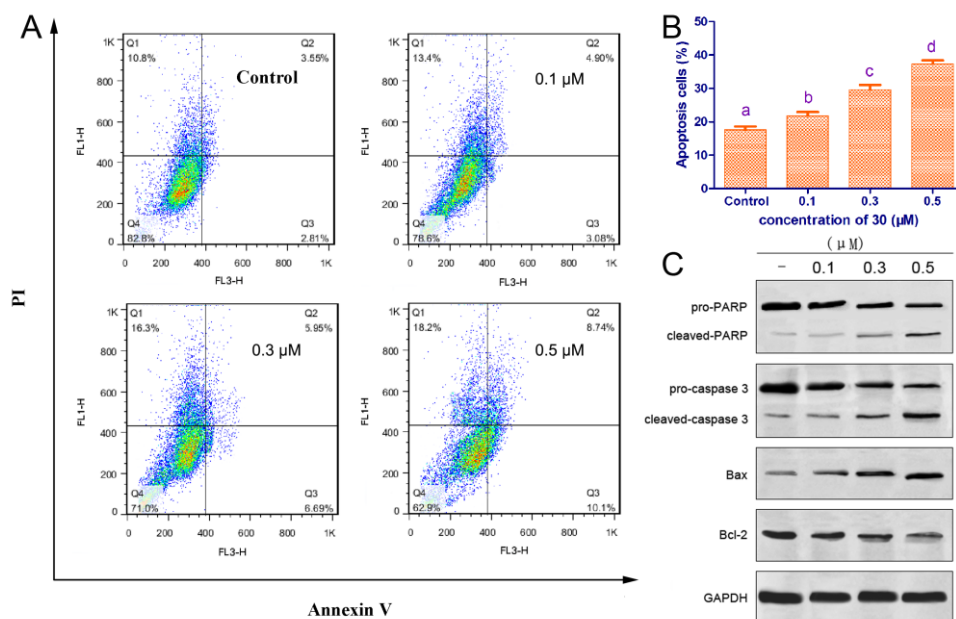


**Fig. 4.** (A) Annexin V/PI dual-immuno-fluorescence staining after treatment with different concentrations of compound **30** revealed significantly increased number of apoptotic and necrotic cells. Cells treated with 0, 0.1, 0.3 and 0.5  $\mu\text{M}$  compound **30** for 24 h were collected and processed for analysis. (B) Apoptosis cells percentage showed in bar diagram. The alphabets a, b, c and d represent the existence of significant difference ( $P < 0.05$ ). (C) Western blot analysis of the levels of the apoptosis-related proteins Bax, PARP, Bcl-2 and Caspase 3 after A549 cells were treated with 0, 0.1, 0.3, 0.5  $\mu\text{M}$  compound **30** for 24 h.

### 2.3.5. Cell cycle analysis [45]

Here, we assessed the cell cycle distribution of A549 cells by flow cytometry after treating with different concentrations (0, 0.1, 0.3, 0.5  $\mu\text{M}$ ) of compound **30** for 24 h. Result indicated that compound **30** arrested cells in the G2/M phase and decreased cells in other phases of the cell cycle (**Fig. 5A** and **5B**). In the vehicle treated group, about 17.62% of A549 cells were distributed in the G2/M phase. Compound **30** increased the proportion of cells in G2/M phase in a concentration-dependent manner (**Fig. 5A** and **5B**). About 22.63%, 28.13%, 40.26%

of cells were distributed in the G2/M phase when treated with 0.1, 0.3, 0.5  $\mu\text{M}$  compound **30** for 24 h respectively.

To explore the further underlying mechanisms of G2/M phase arrest induced by compound **30**, we examined the regulated effect on the expression of several related proteins: cyclin B1, cdc2, cdc25c and P21, which could tightly control the cell cycle progression. Cell arrest at the prometaphase/metaphase to anaphase transition is normally regulated by the mitotic checkpoint. M phase promoting factor (MPF) is the major regulator of the G2 to M transition, which is a complex made up of the catalytic subunit of cdc2 and the regulatory subunit of cyclin B1. They are held in an inactive state by phosphorylation of cdc2 at one negative regulatory site (Tyr15). This and other regulatory complexes are activated at different points during the cell cycle and can also be regulated by several exogenous factors. As shown in **Fig. 5C**, cyclinB1 was slightly up-regulated and cdc25c was down-regulated in a dose-dependent manner. Also, we observed there is a reduction of cdc2 in the dose-dependent manner. Meanwhile, p21 expression increased with compound **30** in a dose-dependent manner.

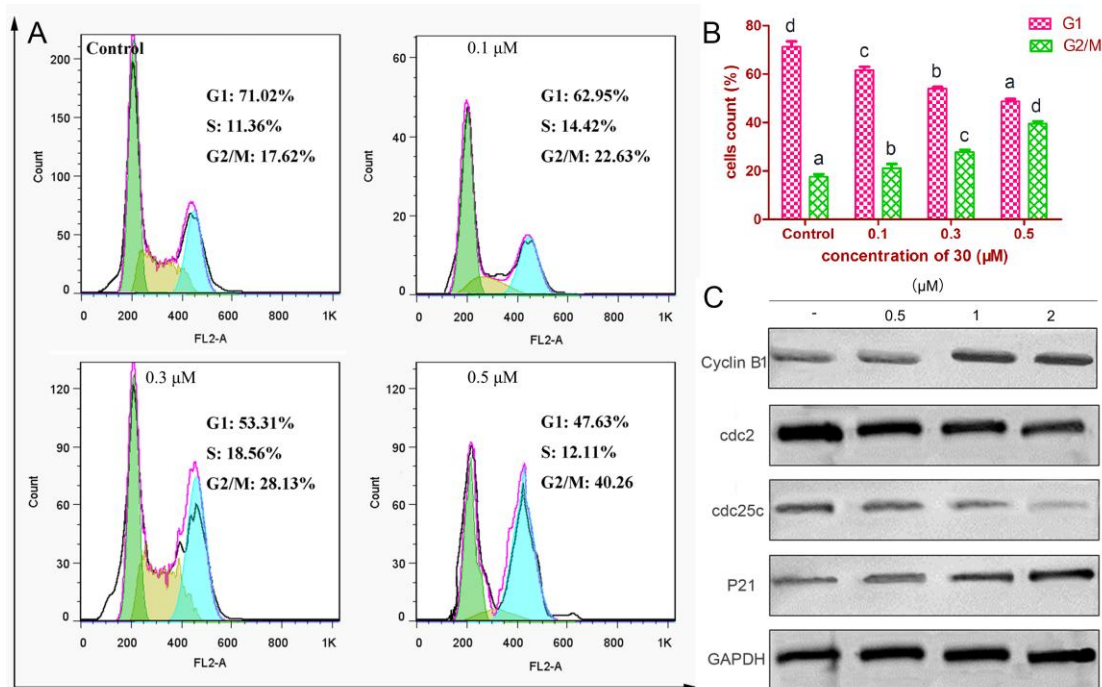


**Fig. 5.** (A) Effect of compound **30** on cell cycle progression of A549 cells was determined by flow cytometry analysis. A549 cells were treated with different concentrations (0.1, 0.3, 0.5  $\mu\text{M}$ ) of compound **30** for 24 h. (B) The percentage of

cells in each cycle phase was indicated. The alphabets a, b, c and d represent the existence of significant difference ( $P < 0.05$ ). (C) Western blot analysis of the levels of the G2/M-related proteins Cyclin B1, cdc25c, cdc2 and P21. A549 cells were treated with 0.1, 0.3, 0.5  $\mu\text{M}$  compound **30** for 24 h.

### 2.3.6. Microtubule disruption and morphological aberrations

Given the importance of the microtubule system in the maintenance of cellular morphology, an assay that involved the disruption of microtubule morphology was performed to reveal whether compound **30** could affect microtubule morphology in living cells. **Fig. 6** clearly showed that regular morphologies of microtubule were turned into a dose-dependent fashion when incubated with compound **30**. The interphase microtubules exhibited fibrous network-like structures in the untreated A549 cells. With the increasing of compound concentration, more cells were found to be contracted and rounded at the dose of 0.2  $\mu\text{M}$ . Besides, when the cells were treated with 0.5  $\mu\text{M}$  compound **30**, spindle microtubules were disorganized and accompanied by misaligned chromosomes from the metaphase plate. These morphological changes of microtubules indicated that compound **30** dramatically disrupts the microtubule morphology, which eventually leads to cell death.

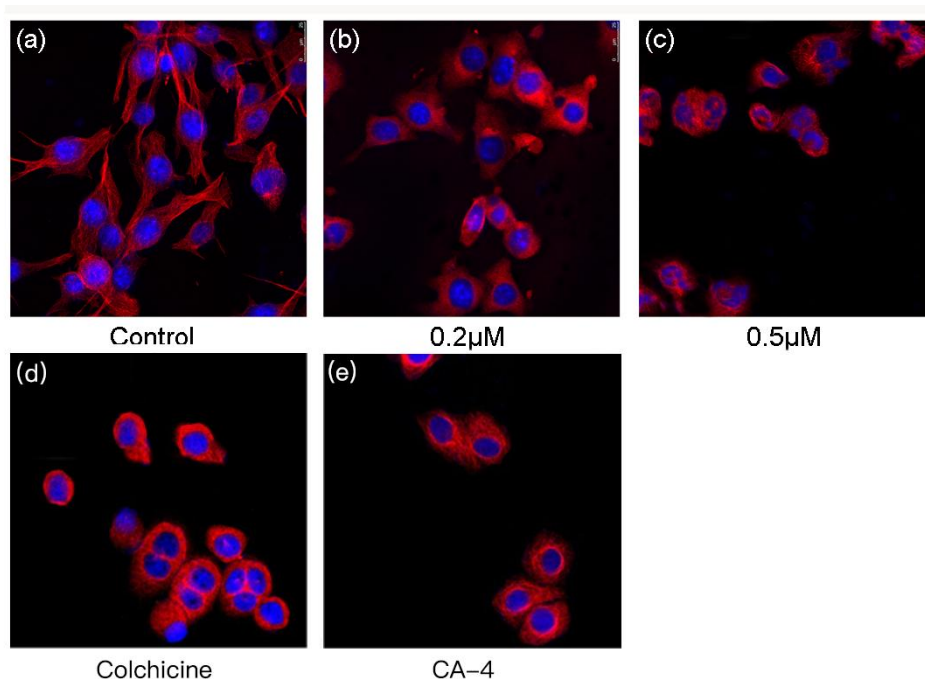


**Fig. 6.** Effects of different concentration of compound **30** (0, 0.2  $\mu\text{M}$ , 0.5  $\mu\text{M}$ ), colchicine (0.2  $\mu\text{M}$ ) and CA-4 (0.2  $\mu\text{M}$ ) on interphase microtubules of A549 cells. Microtubules tagged with rhodamine (red) and nuclei tagged with DAPI (blue) were observed under a confocal microscope. The photomicrographs shown are representative of at least three independent experiments performed.

### 2.3.7. Effects of compounds on tumor volume after treating mouse models of cancer

Based on *in-vitro* experiments, we detect *in-vivo* activity on mouse models of cancer treated with compound **30**, with CA-4 as a contrast. The mouse model was established by intraperitoneal inoculation of rat hepatoma H22 cells in mice. Then the mice model was administered intraperitoneally and the dosage was 3 mg/kg. The results were depicted in **Fig. 7**. As shown in **Fig. 7(a)**, the tumor volumes of the mouse model treated with CA-4 and compound **30** were much smaller than that of the control group; and from eighth to twenty-eighth days, the volume of the tumor after compound **30** treatment was smaller than that of CA-4 treatment. As shown in **Figure 7(b)**, the mouse model treated with compound **30** had no significant weight loss, while the CA-4 treated mouse model decreased more than that of the control group. Therefore, it can be concluded that compound **30** has better anticancer activity than CA-4.

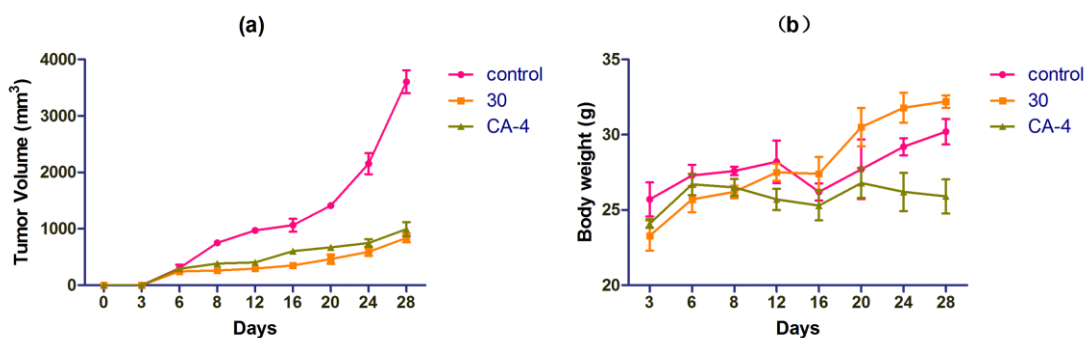


**Fig. 7.** (a) Effects of compound **30** and CA-4 on tumor volume after treating mouse models of cancer. (b) Effects of compound **30** and CA-4 on body weight of mice after treating mouse models of cancer.

## 2.4. Docking simulations

To gain better understanding on the potency of the synthesized compounds and guide further SAR studies, we have proceeded to examine the interaction of the novel 2-(1,3-diphenyl-1H-pyrazol-4-yl)-1-(phenylsulfonyl)-1H-benzo[*d*]imidazole derivatives with tubulin crystal structure (PDB code: 1SA0).

Data of molecular docking simulations for the synthesized compounds **10**, **12-35** were described in **Fig. 8A**, in which the predicted binding interaction energy was used as the criterion for ranking. As depicted in **Fig. 8A**, compounds **15** (−56.09 kcal/mol), **22** (−56.15 kcal/mol), **29** (−56.5 kcal/mol) and **30** (−56.72 kcal/mol) showed lower interaction energy than colchicine (−56.03 kcal/mol), and compound **30** showed the lowest, which means that compound **30** exhibited the most potent affinity for tubulin in prediction.

Then 2D, 3D maps and surface model structure of the most potent compound **30** with 1SA0 were depicted in **Fig. 8** and **Fig. 9** with 2D maps of three comparisons **29**, **22** and **15**. We could see in the figures, all the compounds **30**, **29**, **22** and **15** formed Pi bonds with LYS 254 and LYS 352, and are only different in the interaction position. Compounds **30** and **22** are same in the interaction positions that Pi bonds were formed between ring E and LYS 254 (distance: 3.7 Å, 3.8 Å), and between ring B and LYS 352 (distance: 6.2 Å, 6.2 Å). For compound **29**, one Pi bond was formed between ring B and LYS 254 (distance: 4.7 Å), and the other bond was formed between ring D and LYS 352 (distance: 6.6 Å). While compound **15** formed one Pi bond between ring A and LYS 254 (distance: 5.9 Å), and formed the other Pi bond between ring C and LYS 352 (distance: 6.9 Å). Thus, we could see that compound **30** formed the shortest distance either with LYS 254, or with LYS 352. From the similar interaction we could conclude that these two Pi bonds formed with LYS 254 and LYS 352 are important for the affinity of compound and tubulin. In addition, compound **30** formed a Pi-Sigma bonds between ring C and ASN 258 (distance: 2.8 Å) and two H bonds between two fluorine atoms of ring A and CYS 241 (distance: 4.8 Å, 5.2 Å). Moreover, Compound **22** also formed a Pi-Sigma bonds between ring C and ASN 258

(distance: 2.9 Å), together with a H bond formed between a fluorine atom of ring A and CYS 241 (distance: 4.8 Å).

In addition, we compared the tubulin-docking mode of compound **30** with another compound reported by Romagnoli et al. 2012 [46]. There were similarities between the two combination models. Both formed two hydrogen bonds with LYS 241 and ASN 258, which proved again compound **30** a potent tubulin inhibitor.

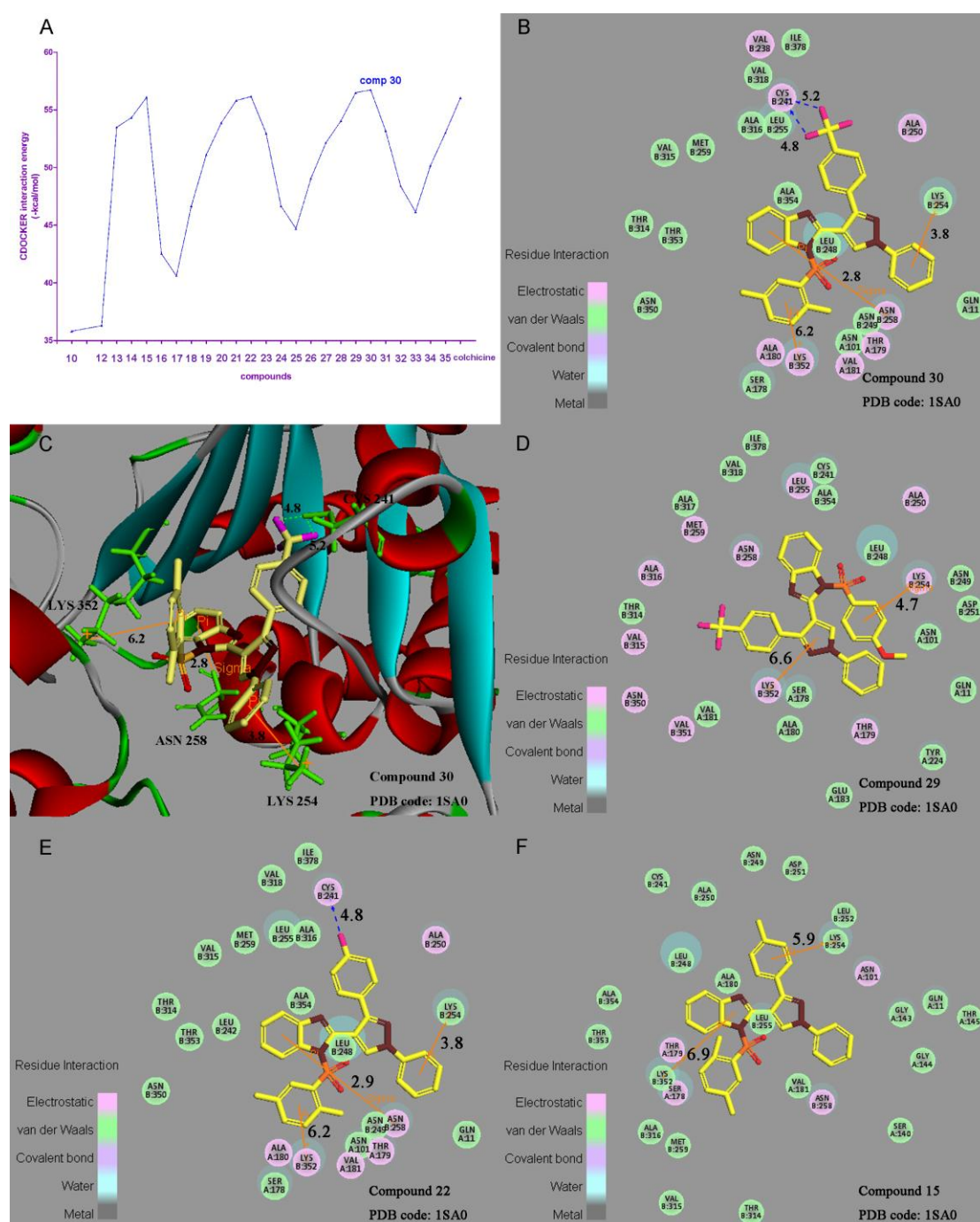


**Fig. 8.** (A) The Cdocker-interaction energy (-kcal/mol) obtained from the docking study of compounds **10**, **12-35** and Colchicine by the CDOCKER protocol. (B-F) The binding mode between the active conformation of compound **30** and the target protein tubulin (PDB code: 1SA0) provided by the CDOCKER protocol (Discovery Studio 3.5, Accelrys, Co. Ltd). (B) 2D molecular docking modeling of compound **30** with 1SA0. (C) 3D model of the interaction between compound **30** and 1SA0 binding site. (D) 2D molecular docking modeling of compound **29** with 1SA0. (E) 2D molecular docking modeling of compound **22** with 1SA0. (F) 2D molecular docking modeling of compound **15** with 1SA0. The hydrogen bonds are displayed as dotted blue arrows and dotted green line, and the Pi-cation bonds are shown as orange lines.

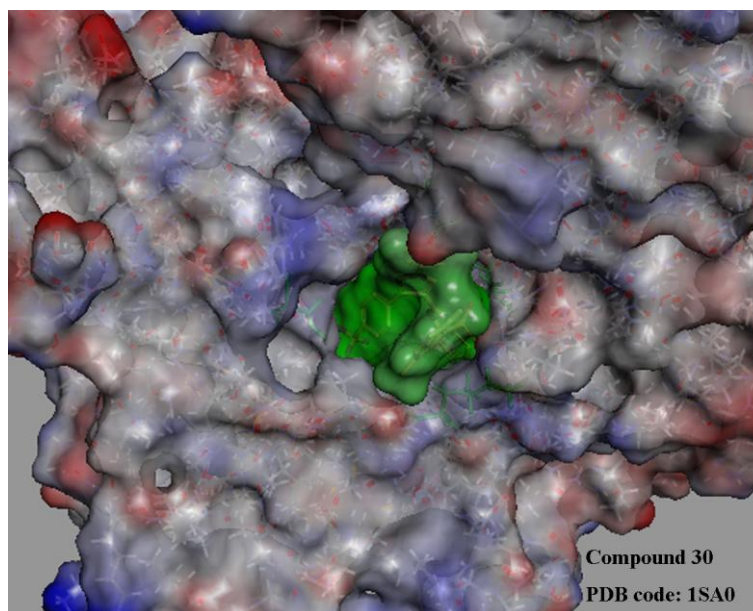


**Fig. 9.** The surface model structure to display the interaction between compound **30** and the targeted protein tubulin.

### 3. Conclusion

twenty-five novel benzimidazole grafted benzulfamide -containing pyrazole ring derivatives were designed and synthesized in this study. Molecular docking simulations were performed by inserting the compounds into the colchicine binding site of tubulin. Compound **30** showed the lowest interaction energy ( $-56.72$  kcal/mol), which means that compound **30** exhibited the most potent affinity for tubulin in prediction. Moreover, these novel compounds showed potent

antiproliferative activities and tubulin polymerization inhibition activities by inserting into colchicine binding site of tubulin; arresting cells in G2/M phase and inducing cell apoptosis. Among these compounds, **30** also showed the most excellent bioactivity. These results strongly suggested that novel benzimidazole grafted benzulfamide-containing pyrazole ring derivatives can be further developed as a promising antitumor agent for the more efficacious treatment of advanced cancers.

## **4. Experimental section**

### **4.1. Materials and measurements**

All chemicals and reagents used in current study were analytical grade. Thin layer chromatography (TLC), proton nuclear magnetic resonance ( $^1\text{H}$  NMR) and elemental microanalyses (CHN) were usually used. Analytical thin-layer chromatography (TLC) was performed on the glass-backed silica gel sheets (silica gel 60 Å GF254). All compounds were detected using UV light (254 nm or 365 nm). Separation of the compounds by column chromatography was carried out with silica gel 60 (200 - 300 mesh ASTM, E. Merck). The quantity of silica gel used was 50-100 times the weight charged on the column. Melting points were determined on a XT4 MP apparatus (Taike Corp., Beijing, China).  $^1\text{H}$  NMR spectra were measured on a Bruker AV-300 or AV-500 spectrometer at 25 °C and referenced to  $\text{Me}_4\text{Si}$ . Chemical shifts are reported in ppm ( $\delta$ ) using the residual solvent line as internal standard. Splitting patterns are designed as s, singlet; d, doublet; t, triplet; m, multiplet. ESI-MS spectra were recorded on a Mariner System 5304 Mass spectrometer. Elemental analyses were performed on a CHN-O-Rapid instrument and were within  $\pm 0.4\%$  of the theoretical values.

### **4.2. General procedure for preparation of 1-phenyl-2-(1-(*p*-tolyl)ethylidene)hydrazine (4)**

*P*-methylacetophenone (compound **1**, 6.71 g, 50 mmol) was added dropwise to a solution of phenylhydrazine hydrochloride (8.68 g, 60 mmol) coupling with sodium acetate (10.21 g, 75 mmol) in water (120 mL). After stirring at room temperature for 3.5 h, a large amount of solid emerged. The yellow precipitate was filtered, washed with water, and dried to give compound **4** (yields 95 %). The corresponding

substituted 1-phenyl-2-(1-phenylethylidene) hydrazines were synthesized following this way to get pure compounds **5** and **6** with a yield of 91% and 96%.

#### **4.3. General procedure for preparation of 1-phenyl-3-(*p*-tolyl)-1*H*-pyrazole-4-carbaldehyde (**7**)**

Compound **4** (8.97 g, 40 mmol) was dissolved in DMF (10 mL), and then was added dropwise to a cold mixed solution of DMF (20 mL) and POCl<sub>3</sub> (10 mL). After stirring at 55 °C for 6 h, the mixture was poured into ice-cold water, with a saturated solution of sodium hydroxide being added to neutralize the mixture. Then a large amount of solid emerged, which was filtered, washed with water, and dried to give compound **7** (yields 91 %). The corresponding substituted 1,3-diphenyl-1*H*-pyrazole-4-carbaldehydes were synthesized following this way to receive pure compounds **8** and **9** with a yield of 88% and 93%.

#### **4.4. General procedure for preparation of 2-(1-phenyl-3-(*p*-tolyl)-1*H*-pyrazol-4-yl)-1*H*-benzo[*d*]imidazole (**10**)**

A solution of *o*-phenylenediamine (3.24 g, 30 mmol) in DMF (20 mL) was added to a suspension of compound **7** (10.51 g, 30 mmol) and sodium pyrosulfite (11.41 g, 60 mmol) in DMF (50 mL). The heterogeneous mixture was stirred at 110 °C for 4 h, then cooled and poured onto a lot of ice. A large amount of solid would emerge, and was filtered to give 2-(1-phenyl-3-(*p*-tolyl)-1*H*-pyrazol-4-yl)-1*H*-benzo[*d*]imidazole (**10**), a yellow powder, yields 83%. The corresponding substituted 2-(1,3-diphenyl-1*H*-pyrazol-4-yl)-1*H*-benzo[*d*]imidazoles were synthesized following this way, and we got pure compounds **11** and **12** with a yield of 82% and 85%.

#### **4.5. General synthesis method of 2-(1-phenyl-3-(*p*-tolyl)-1*H*-pyrazol-4-yl)-1-(phenylsulfonyl)-1*H*-benzo[*d*]imidazole (**13**)**

Compound **13** was synthesized from a stirring mixture of the material compound **10** (0.35 g, 1mmol) and compound **I** (benzenesulfonyl chloride, 0.26 g, 1.5 mmol) with the help of 2 - 3 drops of triethylamine and EDC·HCl (0.21 g, 1.1mmol) in 30 mL dichloromethane at room temperature for 12 h. The reaction mixture was then

extracted with dichloromethane (15 mL × 3) and distilled water (15 mL), and the organic layer was concentrated under vacuum to get the crude product. The crude product was purified by silica gel column chromatography (200 - 300 mesh) eluted with a mixture of ethyl acetate and petroleum ether (v/v = 1:8) to afford pure product (compound **13**, yields 71 %). The corresponding substituted 2-(1,3-diphenyl-1*H*-pyrazol-4-yl)-1-(phenylsulfonyl)-1*H*-benzo[*d*]imidazoles compounds were synthesized following this way, and we got pure compounds **14 - 35** with yields of 69 - 87%.

#### **4.5.1 2-(1-phenyl-3-(*p*-tolyl)-1*H*-pyrazol-4-yl)-1-(phenylsulfonyl)-1*H*-benzo[*d*]imidazole (13)**

Yellow powder, yield: 80%. M. p: 235 - 236 °C, <sup>1</sup>H NMR (DMSO-*d*<sub>6</sub>, 400 MHz) δ: 2.38 (s, 3H); 7.31 - 7.32 (m, 5H); 7.48 - 7.51 (m, 1H); 7.57 - 7.66 (m, 8H); 7.81 - 7.83 (m, 2H); 7.96 - 7.98 (m, 2H); 9.30 (s, 1H). <sup>13</sup>C NMR (DMSO-*d*<sub>6</sub>, 100 MHz) δ: 21.38, 114.54, 119.54, 125.91, 126.31, 128.15, 128.25, 128.37, 128.99, 130.09, 130.44, 132.32, 133.32, 138.98, 139.46, 143.97, 151.56. ESI-MS: 490.58 (C<sub>29</sub>H<sub>22</sub>N<sub>4</sub>O<sub>2</sub>S, [M+H]<sup>+</sup>). Anal. Calcd for C<sub>29</sub>H<sub>22</sub>N<sub>4</sub>O<sub>2</sub>S: C, 71.00; H, 4.52; N, 11.42; O, 6.52; S, 6.54; Found: C, 71.02; H, 4.54; N, 11.45.

#### **4.5.2 2-(1-phenyl-3-(*p*-tolyl)-1*H*-pyrazol-4-yl)-1-tosyl-1*H*-benzo[*d*]imidazole (14)**

White powder, yield: 88%. M. p: 242 - 244 °C, <sup>1</sup>H NMR (DMSO-*d*<sub>6</sub>, 400 MHz) δ: 2.27 (s, 3H); 2.37 (s, 3H); 7.11 (d, *J* = 7.6, 2H); 7.3 (d, *J* = 8, 2H); 7.46 - 7.50 (m, 3H); 7.56 - 7.59 (m, 4H); 7.61 - 7.65 (m, 2H); 7.79 - 7.81 (m, 2H); 7.96 (d, *J* = 0.8, 2H); 9.25 (s, 1H). <sup>13</sup>C NMR (DMSO-*d*<sub>6</sub>, 100 MHz) δ: 21.21, 21.35, 105.83, 114.52, 119.58, 125.91, 126.24, 128.16, 128.20, 128.40, 128.67, 130.08, 130.43, 132.46, 133.07, 138.62, 138.94, 139.50, 143.98, 145.33, 151.60. ESI-MS: 504.60 (C<sub>30</sub>H<sub>24</sub>N<sub>4</sub>O<sub>2</sub>S, [M+H]<sup>+</sup>). Anal. Calcd for C<sub>30</sub>H<sub>24</sub>N<sub>4</sub>O<sub>2</sub>S: C, 71.41; H, 4.79; N, 11.10; O, 6.34; S, 6.35; Found: C, 71.41; H, 4.73; N, 11.10.

#### **4.5.3 1-((2,5-dimethylphenyl)sulfonyl)-2-(1-phenyl-3-(*p*-tolyl)-1*H*-pyrazol-4-yl)-1*H*-benzo[*d*]imidazole (15)**

White powder, yield: 76%. M. p: 227 - 228 °C, <sup>1</sup>H NMR (DMSO-*d*<sub>6</sub>, 400 MHz) δ: 2.23 (s, 3H); 2.38 (s, 3H); 2.46 (s, 3H); 7.00 (s, 2H); 7.30 - 7.32 (m, 2H); 7.46 -

7.50 (m, 1H); 7.55 - 7.66 (m, 7H); 7.80 - 7.82 (m, 2H); 7.96 - 7.98 (m, 2H); 9.28 (s, 1H). <sup>13</sup>C NMR (DMSO-*d*<sub>6</sub>, 100 MHz)  $\delta$ : 20.09, 21.01, 21.38, 105.75, 114.54, 119.54, 126.27, 127.53, 128.24, 128.37, 129.54, 130.08, 130.43, 131.06, 132.40, 132.75, 133.25, 134.05, 138.97, 139.46, 143.98, 146.20, 151.55. ESI-MS: 518.63 (C<sub>31</sub>H<sub>26</sub>N<sub>4</sub>O<sub>2</sub>S, [M+H]<sup>+</sup>). Anal. Calcd for C<sub>31</sub>H<sub>26</sub>N<sub>4</sub>O<sub>2</sub>S: C, 71.79; H, 5.05; N, 10.80; O, 6.17; S, 6.18; Found: C, 71.77; H, 5.04; N, 10.80.

**4.5.4 1-((4-fluorophenyl)sulfonyl)-2-(1-phenyl-3-(p-tolyl)-1H-pyrazol-4-yl)-1H-benzo[*d*]imidazole (16)**

White powder, yield: 77%. M. p: 244 - 245 °C, <sup>1</sup>H NMR (DMSO-*d*<sub>6</sub>, 400 MHz)  $\delta$ : 2.25 (s, 3H); 7.03 - 7.18 (m, 2H); 7.20 - 7.43 (m, 4H); 7.45 - 7.65 (m, 7H); 7.81 - 7.83 (m, 1H); 7.98 - 8.00 (m, 2H); 8.13 - 8.15 (m, 1H); 8.97 (s, 1H). <sup>13</sup>C NMR (DMSO-*d*<sub>6</sub>, 100 MHz)  $\delta$ : 21.37, 105.90, 114.56, 114.79, 114.94, 115.71, 119.54, 126.22, 128.24, 128.28, 128.34, 128.37, 130.07, 130.45, 132.53, 133.19, 138.99, 139.45, 144.04, 145.14, 145.16, 151.55. ESI-MS: 508.57 (C<sub>29</sub>H<sub>21</sub>FN<sub>4</sub>O<sub>2</sub>S, [M+H]<sup>+</sup>). Anal. Calcd for C<sub>29</sub>H<sub>21</sub>FN<sub>4</sub>O<sub>2</sub>S: C, 68.49; H, 4.16; N, 11.02; O, 6.29; S, 6.30; Found: C, 68.45; H, 4.15; N, 11.02.

**4.5.5 1-((4-chlorophenyl)sulfonyl)-2-(1-phenyl-3-(p-tolyl)-1H-pyrazol-4-yl)-1H-benzo[*d*]imidazole (17)**

White powder, yield: 81%. M. p: 254 - 256 °C, <sup>1</sup>H NMR (DMSO-*d*<sub>6</sub>, 400 MHz)  $\delta$ : 2.32 (s, 3H); 7.26 - 7.29 (m, 2H); 7.31 - 7.35 (m, 2H); 7.51 - 7.55 (m, 2H); 7.63 - 7.65 (m, 6H); 7.83 - 7.85 (m, 5H); 8.36 (s, 1H). ESI-MS: 525.02 (C<sub>29</sub>H<sub>21</sub>ClN<sub>4</sub>O<sub>2</sub>S, [M+H]<sup>+</sup>). Anal. Calcd for C<sub>29</sub>H<sub>21</sub>ClN<sub>4</sub>O<sub>2</sub>S: C, 66.34; H, 4.03; N, 10.67; O, 6.09; S, 6.11; Found: C, 66.34; H, 4.053; N, 10.65.

**4.5.6 1-((4-bromophenyl)sulfonyl)-2-(1-phenyl-3-(p-tolyl)-1H-pyrazol-4-yl)-1H-benzo[*d*]imidazole (18)**

Yellow powder, yield: 82%. M. p: 235 - 236 °C, <sup>1</sup>H NMR (DMSO-*d*<sub>6</sub>, 400 MHz)  $\delta$ : 2.38 (s, 3H); 7.31 (d, *J* = 8, 2H); 7.47 - 7.55 (m, 5H); 7.58 - 7.66 (m, 6H); 7.82 - 7.84 (m, 2H); 7.95 - 7.98 (m, 2H); 9.28 (s, 1H). <sup>13</sup>C NMR (DMSO-*d*<sub>6</sub>, 100 MHz)  $\delta$ : 21.37, 105.40, 114.49, 119.11, 119.60, 122.30, 126.48, 127.26, 128.11, 128.44, 129.59, 130.13, 130.45, 131.16, 132.06, 133.30, 138.94, 139.55, 143.88, 147.68,

151.62. ESI-MS: 569.47 (C<sub>29</sub>H<sub>21</sub>BrN<sub>4</sub>O<sub>2</sub>S, [M+H]<sup>+</sup>). Anal. Calcd for C<sub>29</sub>H<sub>21</sub>BrN<sub>4</sub>O<sub>2</sub>S: C, 61.16; H, 3.72; N, 9.84; O, 5.62; S, 5.63; Found: C, 61.16; H, 3.75; N, 9.83.

**4.5.7 2-(1-phenyl-3-(p-tolyl)-1H-pyrazol-4-yl)-1-((4-(trifluoromethyl)phenyl)sulfonyl)-1H-benzo[d]imidazole (19)**

White powder, yield: 85%. M. p: 247 - 248 °C, <sup>1</sup>H NMR (DMSO-*d*<sub>6</sub>, 400 MHz)  $\delta$ : 2.38 (s, 3H); 7.31 (d, *J* = 8, 2H); 7.46 - 7.50 (m, 1H); 7.56 - 7.66 (m, 6H); 7.69 - 7.71 (m, 2H); 7.80 - 7.83 (m, 4H); 7.96 - 7.98 (m, 2H); 9.26 (s, 1H). <sup>13</sup>C NMR (DMSO-*d*<sub>6</sub>, 100 MHz)  $\delta$ : 21.36, 105.85, 114.55, 119.55, 125.39, 125.42, 125.44, 126.24, 126.80, 128.23, 128.38, 129.24, 129.45, 130.08, 130.45, 132.49, 133.18, 138.98, 139.46, 144.03, 151.56, 152.37. ESI-MS: 558.57 (C<sub>30</sub>H<sub>21</sub>F<sub>3</sub>N<sub>4</sub>O<sub>2</sub>S, [M+H]<sup>+</sup>). Anal. Calcd for C<sub>30</sub>H<sub>21</sub>F<sub>3</sub>N<sub>4</sub>O<sub>2</sub>S: C, 64.51; H, 3.79; N, 10.03; O, 5.73; S, 5.74; Found: C, 64.55; H, 3.79; N, 10.03.

**4.5.8 2-(3-(4-fluorophenyl)-1-phenyl-1H-pyrazol-4-yl)-1-(phenylsulfonyl)-1H-benzo[d]imidazole (20)**

Yellow powder, yield: 68%. M. p: 227 - 228 °C, <sup>1</sup>H NMR (DMSO-*d*<sub>6</sub>, 400 MHz)  $\delta$ : 7.30 - 7.33 (m, 5H); 7.35 - 7.37 (m, 2H); 7.60 - 7.64 (m, 5H); 7.78 - 7.84 (m, 4H); 7.96 - 7.99 (m, 2H); 9.32 (s, 1H). <sup>13</sup>C NMR (DMSO-*d*<sub>6</sub>, 100 MHz)  $\delta$ : 19.00, 56.51, 114.51, 116.48, 116.62, 119.62, 125.91, 126.44, 128.17, 128.51, 128.83, 129.05, 129.85, 130.22, 130.46, 130.72, 130.78, 132.13, 133.44, 138.89, 143.68, 148.41, 150.69, 162.53, 164.16. ESI-MS: 494.54 (C<sub>28</sub>H<sub>19</sub>FN<sub>4</sub>O<sub>2</sub>S, [M+H]<sup>+</sup>). Anal. Calcd for C<sub>28</sub>H<sub>19</sub>FN<sub>4</sub>O<sub>2</sub>S: C, 68.00; H, 3.87; N, 11.33; O, 6.47; S, 6.48; Found: C, 68.00; H, 3.85; N, 11.37.

**4.5.9 2-(3-(4-fluorophenyl)-1-phenyl-1H-pyrazol-4-yl)-1-((4-methoxyphenyl)sulfonyl)-1H-benzo[d]imidazole (21)**

White powder, yield: 82%. M. p: 231 - 232 °C, <sup>1</sup>H NMR (DMSO-*d*<sub>6</sub>, 400 MHz)  $\delta$ : 3.74 (s, 3H); 6.83 - 6.85 (m, 2H); 7.32 - 7.36 (m, 2H); 7.47 - 7.50 (m, 1H); 7.52 - 7.55 (m, 2H); 7.56 - 7.58 (m, 2H); 7.62 - 7.66 (m, 2H); 7.77 - 7.82 (m, 4H); 7.97 - 7.98 (m, 2H); 9.29 (s, 1H). <sup>13</sup>C NMR (DMSO-*d*<sub>6</sub>, 100 MHz)  $\delta$ : 18.98, 55.60, 56.52, 106.14, 113.27, 114.55, 116.41, 116.56, 119.59, 126.18, 127.51, 127.62, 127.64, 128.45, 130.44, 130.72, 130.78, 132.59, 133.24, 138.92, 140.90, 143.83, 150.64,

159.82, 162.48, 164.11. ESI-MS: 524.57 ( $C_{29}H_{21}FN_4O_3S$ ,  $[M+H]^+$ ). Anal. Calcd for  $C_{29}H_{21}FN_4O_3S$ : C, 66.40; H, 4.04; N, 10.68; O, 9.15; S, 6.11; Found: C, 66.40; H, 4.05; N, 10.63.

**4.5.10 1-((2,5-dimethylphenyl)sulfonyl)-2-(3-(4-fluorophenyl)-1-phenyl-1H-pyrazol-4-yl)-1H-benzo[d]imidazole (22)**

White powder, yield: 74%. M. p: 242 - 243 °C,  $^1H$  NMR (DMSO- $d_6$ , 400 MHz)  $\delta$ : 2.22 (s, 3H); 2.45 (s, 3H); 7.00 (s, 2H); 7.31 - 7.36 (s, 2H); 7.47 - 7.50 (s, 1H); 7.54 - 7.58 (m, 3H); 7.61 - 7.65 (m, 2H); 7.75 - 7.80 (m, 4H); 7.95 - 7.97 (m, 2H); 9.24 (s, 1H).  $^{13}C$  NMR (DMSO- $d_6$ , 100 MHz)  $\delta$ : 20.06, 20.99, 106.14, 113.27, 114.52, 116.38, 116.59, 119.62, 126.18, 127.51, 128.50, 129.66, 130.45, 130.70, 130.79, 131.13, 132.55, 132.77, 133.12, 134.13, 138.89, 143.70, 145.94, 150.66. ESI-MS: 522.59 ( $C_{30}H_{23}FN_4O_2S$ ,  $[M+H]^+$ ). Anal. Calcd for  $C_{30}H_{23}FN_4O_2S$ : C, 68.95; H, 4.44; N, 10.72; O, 6.12; S, 6.14; Found: C, 68.95; H, 4.43; N, 10.76.

**4.5.11 4-((2-(3-(4-fluorophenyl)-1-phenyl-1H-pyrazol-4-yl)-1H-benzo[d]imidazole-1-yl)sulfonyl)phenyl nitrate (23)**

Yellow powder, yield: 89%. M. p: 252 - 253 °C,  $^1H$  NMR (DMSO- $d_6$ , 400 MHz)  $\delta$ : 7.32 - 7.37 (m, 2H); 7.47 - 7.51 (m, 1H); 7.56 - 7.58 (m, 2H); 7.62 - 7.66 (m, 2H); 7.77 - 7.85 (m, 6H); 7.96 - 7.98 (m, 2H); 8.19 (d,  $J = 8.8$ , 2H); 9.27 (s, 1H).  $^{13}C$  NMR (DMSO- $d_6$ , 100 MHz)  $\delta$ : 18.97, 56.52, 106.19, 114.55, 116.42, 116.56, 119.60, 123.83, 126.18, 127.38, 127.62, 127.63, 128.48, 130.46, 130.71, 130.77, 132.64, 133.18, 138.92, 143.85, 147.78, 150.64, 154.43, 162.48, 164.11. ESI-MS: 555.54 ( $C_{28}H_{18}FN_5O_5S$ ,  $[M+H]^+$ ). Anal. Calcd for  $C_{28}H_{18}FN_5O_5S$ : C, 60.54; H, 3.27; N, 12.61; O, 14.40; S, 5.77; Found: C, 60.56; H, 3.25; N, 12.63.

**4.5.12 2-(3-(4-fluorophenyl)-1-phenyl-1H-pyrazol-4-yl)-1-((4-fluorophenyl)sulfonyl)-1H-benzo[d]imidazole (24)**

Yellow powder, yield: 77%. M. p: 228 - 229 °C,  $^1H$  NMR (DMSO- $d_6$ , 400 MHz)  $\delta$ : 7.10 - 7.15 (m, 2H); 7.31 - 7.49 (m, 2H); 7.49 - 7.58 (m, 1H); 7.59 - 7.62 (m, 2H); 7.63 - 7.66 (m, 4H); 7.75 - 7.82 (m, 4H); 7.95 - 7.97 (m, 2H); 9.24 (s, 1H).  $^{13}C$  NMR (DMSO- $d_6$ , 100 MHz)  $\delta$ : 18.87, 56.47, 105.71, 114.47, 115.03, 116.46, 116.60, 119.65, 126.41, 127.48, 128.31, 130.45, 132.13, 133.28, 138.87, 143.56, 144.64,

144.66, 150.71, 161.72, 162.50, 163.35. ESI-MS: 512.53 (C<sub>28</sub>H<sub>18</sub>F<sub>2</sub>N<sub>4</sub>O<sub>2</sub>S, [M+H]<sup>+</sup>). Anal. Calcd for C<sub>28</sub>H<sub>18</sub>F<sub>2</sub>N<sub>4</sub>O<sub>2</sub>S: C, 65.62; H, 3.54; N, 10.93; O, 6.24; S, 6.26; Found: C, 65.64; H, 3.56; N, 10.92.

**4.5.13 1-((4-chlorophenyl)sulfonyl)-2-(3-(4-fluorophenyl)-1-phenyl-1H-pyrazol-4-yl)-1H-benzo[d]imidazole (25)**

Yellow powder, yield: 82%. M. p: 257 - 258 °C, <sup>1</sup>H NMR (DMSO-*d*<sub>6</sub>, 400 MHz) δ: 7.28 - 7.36 (m, 4H); 7.52 - 7.56 (m, 2H); 7.66 - 7.68 (m, 4H); 7.77 - 7.81 (m, 2H); 7.84 - 7.86 (m, 5H); 8.42 (s, 1H). <sup>13</sup>C NMR (DMSO-*d*<sub>6</sub>, 100 MHz) δ: 18.92, 56.53, 115.88, 116.01, 116.04, 116.19, 118.51, 119.72, 128.99, 129.77, 129.83, 130.05, 130.15, 130.20, 130.25, 130.75, 130.88, 131.32, 131.37, 137.12, 140.56, 147.14. ESI-MS: 528.98 (C<sub>28</sub>H<sub>18</sub>ClFN<sub>4</sub>O<sub>2</sub>S, [M+H]<sup>+</sup>). Anal. Calcd for C<sub>28</sub>H<sub>18</sub>ClFN<sub>4</sub>O<sub>2</sub>S: C, 63.57; H, 3.43; N, 10.59; O, 6.05; S, 6.06; Found: C, 63.54; H, 3.43; N, 10.56.

**4.5.14 1-((4-bromophenyl)sulfonyl)-2-(3-(4-fluorophenyl)-1-phenyl-1H-pyrazol-4-yl)-1H-benzo[d]imidazole (26)**

Yellow powder, yield: 83%. M. p: 261 - 262 °C, <sup>1</sup>H NMR (DMSO-*d*<sub>6</sub>, 400 MHz) δ: 7.32 - 7.37 (m, 2H); 7.51 - 7.58 (m, 4H); 7.58 - 7.60 (m, 2H); 7.62 - 7.66 (m, 3H); 7.76 - 7.80 (m, 2H); 7.81 - 7.83 (m, 2H); 7.96 - 9.98 (m, 2H); 9.31 (s, 1H). <sup>13</sup>C NMR (DMSO-*d*<sub>6</sub>, 100 MHz) δ: 19.00, 56.51, 105.73, 114.52, 116.46, 116.61, 119.61, 122.27, 126.40, 127.54, 127.56, 128.18, 128.49, 130.29, 130.33, 130.34, 130.45, 130.71, 130.77, 131.14, 132.20, 133.40, 138.90, 143.71, 147.76, 150.68, 162.52, 164.15. ESI-MS: 573.44 (C<sub>28</sub>H<sub>18</sub>BrFN<sub>4</sub>O<sub>2</sub>S, [M+H]<sup>+</sup>). Anal. Calcd for C<sub>28</sub>H<sub>18</sub>BrFN<sub>4</sub>O<sub>2</sub>S: C, 58.65; H, 3.16; N, 9.77; O, 5.58; S, 5.59; Found: C, 58.64; H, 3.13; N, 9.76.

**4.5.15 2-(3-(4-fluorophenyl)-1-phenyl-1H-pyrazol-4-yl)-1-((4-(trifluoromethyl)phenyl)sulfonyl)-1H-benzo[d]imidazole (27)**

White powder, yield: 84%. M. p: 243 - 244 °C, <sup>1</sup>H NMR (DMSO-*d*<sub>6</sub>, 400 MHz) δ: 7.32 - 7.37 (m, 2H); 7.47 - 7.51 (m, 1H); 7.55 - 7.57 (m, 2H); 7.62 - 7.66 (m, 2H); 7.69 - 7.71 (m, 2H); 7.78 - 7.82 (m, 6H); 7.96 - 7.98 (m, 2H); 9.28 (s, 1H). <sup>13</sup>C NMR (DMSO-*d*<sub>6</sub>, 100 MHz) δ: 19.00, 56.50, 114.57, 116.39, 116.60, 116.58, 125.38, 125.42, 126.17, 126.79, 128.47, 130.47, 130.71, 130.79, 133.24, 138.92, 150.62.

ESI-MS: 562.54 (C<sub>29</sub>H<sub>18</sub>F<sub>4</sub>N<sub>4</sub>O<sub>2</sub>S: [M+H]<sup>+</sup>). Anal. Calcd for C<sub>29</sub>H<sub>18</sub>F<sub>4</sub>N<sub>4</sub>O<sub>2</sub>S: C, 61.92; H, 3.23; N, 9.96; O, 5.69; S, 5.70; Found: C, 61.95; H, 3.23; N, 9.92.

**4.5.16 2-(1-phenyl-3-(4-(trifluoromethyl)phenyl)-1H-pyrazol-4-yl)-1-(phenylsulfonyl)-1H-benzo[d]imidazole (28)**

White powder, yield: 80%. M. p: 232 - 233 °C, <sup>1</sup>H NMR (DMSO-*d*<sub>6</sub>, 400 MHz) δ: 7.30 - 7.32 (m, 3H); 7.48 - 7.52 (m, 1H); 7.57 - 7.59 (m, 2H); 7.61 - 7.67 (m, 4H); 7.81 - 7.84 (m, 2H); 7.86 - 7.88 (m, 2H); 7.97 - 8.00 (m, 4H); 9.38 (s, 1H). <sup>13</sup>C NMR (DMSO-*d*<sub>6</sub>, 100 MHz) δ: 106.46, 114.61, 119.72, 119.79, 123.73, 125.54, 125.90, 126.30, 126.39, 126.42, 128.19, 128.65, 128.76, 129.13, 129.23, 129.80, 129.85, 129.90, 130.01, 130.47, 132.52, 133.68, 135.21, 138.85, 143.51, 148.26, 150.06. ESI-MS: 544.55 (C<sub>29</sub>H<sub>19</sub>F<sub>3</sub>N<sub>4</sub>O<sub>2</sub>S, [M+H]<sup>+</sup>). Anal. Calcd for C<sub>29</sub>H<sub>19</sub>F<sub>3</sub>N<sub>4</sub>O<sub>2</sub>S: C, 63.96; H, 3.52; N, 10.29; O, 5.88; S, 5.89; Found: C, 63.93; H, 3.54; N, 10.26.

**4.5.17 1-((4-methoxyphenyl)sulfonyl)-2-(1-phenyl-3-(4-(trifluoromethyl)phenyl)-1H-pyrazol-4-yl)-1H-benzo[d]imidazole (29)**

Yellow powder, yield: 79%. M. p: 244 - 246 °C, <sup>1</sup>H NMR (DMSO-*d*<sub>6</sub>, 400 MHz) δ: 3.73 (s, 3H); 6.82 - 6.85 (m, 2H); 7.53 - 7.58 (m, 3H); 7.59 - 7.60 (m, 2H); 7.63 - 7.67 (m, 2H); 7.82 - 7.83 (m, 2H); 7.84 - 7.88 (m, 2H); 7.95 - 8.00 (m, 4H); 9.38 (s, 1H). <sup>13</sup>C NMR (DMSO-*d*<sub>6</sub>, 100 MHz) δ: 55.58, 106.18, 113.30, 114.57, 119.72, 123.28, 125.98, 126.43, 127.50, 128.67, 129.22, 129.76, 130.08, 130.47, 132.25, 133.78, 135.13, 138.82, 140.67, 143.41, 150.08, 159.87. ESI-MS: 574.57 (C<sub>30</sub>H<sub>21</sub>F<sub>3</sub>N<sub>4</sub>O<sub>3</sub>S, [M+H]<sup>+</sup>). Anal. Calcd for C<sub>30</sub>H<sub>21</sub>F<sub>3</sub>N<sub>4</sub>O<sub>3</sub>S: C, 62.71; H, 3.68; N, 9.75; O, 8.35; S, 5.58; Found: C, 62.75; H, 3.63; N, 9.75.

**4.5.18 1-((2,5-dimethylphenyl)sulfonyl)-2-(1-phenyl-3-(4-(trifluoromethyl)phenyl)-1H-pyrazol-4-yl)-1H-benzo[d]imidazole (30)**

Yellow powder, yield: 83%. M. p: 255 - 257 °C, <sup>1</sup>H NMR (DMSO-*d*<sub>6</sub>, 400 MHz) δ: 2.22 (s, 3H); 2.45 (s, 3H); 7.00 (s, 2H); 7.48 - 7.55 (m, 2H); 7.56 - 7.57 (m, 2H); 7.62 - 7.66 (m, 2H); 7.78 - 7.81 (m, 2H); 7.84 - 7.86 (m, 2H); 7.95 - 7.96 (m, 4H); 9.28 (s, 1H). <sup>13</sup>C NMR (DMSO-*d*<sub>6</sub>, 100 MHz) δ: 18.85, 20.05, 20.98, 106.90, 114.61, 119.74, 123.71, 125.51, 126.08, 126.35, 126.37, 127.51, 128.66, 129.21, 129.56, 129.69, 129.77, 129.99, 130.20, 130.48, 131.15, 132.78, 132.91, 133.35, 134.14,

135.23, 138.85, 143.53, 145.89, 150.05. ESI-MS: 572.60 ( $C_{31}H_{23}F_3N_4O_2S:[M+H]^+$ ).  
Anal. Calcd for  $C_{31}H_{23}F_3N_4O_2S$ : C, 65.02; H, 4.05; N, 9.78; O, 5.59; S, 5.60; Found:  
C, 65.05; H, 4.03; N, 9.76.

**4.5.19 4-((2-(1-phenyl-3-(4-(trifluoromethyl)phenyl)-1H-pyrazol-4-yl)-1H-benzo[d]imidazol-1-yl)sulfonyl)phenyl nitrate (31)**

Yellow powder, yield: 86%. M. p: 212 - 213 °C,  $^1H$  NMR (DMSO- $d_6$ , 400 MHz)  
 $\delta$ : 7.58 - 7.61 (m, 3H); 7.82 - 7.85 (m, 6H); 7.96 - 8.00 (m, 4H); 8.18 - 8.20 (m, 4H);  
9.33 (s, 1H).  $^{13}C$  NMR (DMSO- $d_6$ , 100 MHz)  $\delta$ : 31.14, 106.30, 114.58, 119.75,  
123.84, 126.42, 127.37, 127.94, 128.72, 129.21, 129.95, 130.07, 130.51, 132.26,  
133.66, 134.56, 135.13, 138.82, 143.44, 147.79, 150.08, 154.38. ESI-MS: 605.54  
( $C_{29}H_{18}F_3N_5O_5S, [M+H]^+$ ). Anal. Calcd for  $C_{29}H_{18}F_3N_5O_5S$ : C, 57.52; H, 3.00; N,  
11.57; O, 13.21; S, 5.30; Found: C, 57.57; H, 3.03; N, 11.52.

**4.5.20 1-((4-fluorophenyl)sulfonyl)-2-(1-phenyl-3-(4-(trifluoromethyl)phenyl)-1H-pyrazol-4-yl)-1H-benzo[d]imidazole (32)**

White powder, yield: 89%. M. p: 221 - 223 °C,  $^1H$  NMR (DMSO- $d_6$ , 400 MHz)  
 $\delta$ : 7.19 - 7.23 (m, 2H); 7.44 - 7.48 (m, 1H); 7.51 - 7.58 (m, 4H); 7.61 - 7.66 (m, 6H);  
7.84 - 7.86 (m, 1H); 8.00 - 8.03 (m, 2H); 8.16 - 8.18 (s, 1H); 9.05 (s, 1H).  $^{13}C$  NMR  
(DMSO- $d_6$ , 100 MHz)  $\delta$ : 106.62, 114.63, 114.82, 114.97, 119.71, 125.54, 126.23,  
126.38, 126.41, 128.29, 128.34, 128.65, 129.23, 129.79, 130.00, 130.49, 132.67,  
133.62, 135.23, 138.86, 143.56, 144.99, 145.01, 150.04, 161.65, 163.27. ESI-MS:  
562.54 ( $C_{29}H_{18}F_4N_4O_2S: [M+H]^+$ ). Anal. Calcd for  $C_{29}H_{18}F_4N_4O_2S$ : C, 61.92; H, 3.23;  
N, 9.96; O, 5.69; S, 5.70; Found: C, 61.95; H, 3.26; N, 9.93.

**4.5.21 1-((4-chlorophenyl)sulfonyl)-2-(1-phenyl-3-(4-(trifluoromethyl)phenyl)-1H-pyrazol-4-yl)-1H-benzo[d]imidazole (33)**

Yellow powder, yield: 77%. M. p: 219 - 221 °C,  $^1H$  NMR (DMSO- $d_6$ , 400 MHz)  
 $\delta$ : 7.35 - 7.38 (m, 2H); 7.49 - 7.52 (m, 1H); 7.57 - 7.60 (m, 1H); 7.61 - 7.63 (m, 2H);  
7.65 - 7.67 (m, 2H); 7.81 - 7.84 (m, 2H); 7.85 - 7.87 (m, 2H); 7.96 - 8.00 (m, 5H);  
9.34 (s, 1H).  $^{13}C$  NMR (DMSO- $d_6$ , 100 MHz)  $\delta$ : 106.47, 114.60, 119.71, 125.98,  
126.31, 126.39, 127.89, 128.23, 128.67, 129.22, 129.74, 130.06, 130.49, 132.52,  
133.64, 135.19, 138.83, 143.50, 147.25, 150.05. ESI-MS: 578.99 ( $C_{29}H_{18}ClF_3N_4O_2S$ :

[M+H]<sup>+</sup>). Anal. Calcd for C<sub>29</sub>H<sub>18</sub>ClF<sub>3</sub>N<sub>4</sub>O<sub>2</sub>S: C, 60.16; H, 3.13; N, 9.68; O, 5.53; S, 5.54; Found: C, 60.15; H, 3.13; N, 9.65.

#### 4.5.22 1-((4-bromophenyl)sulfonyl)-2-(1-phenyl-3-(4-(trifluoromethyl)phenyl)-1H-pyrazol-4-yl)-1H-benzo[d]imidazole (34)

White powder, yield: 82%. M. p: 254 - 256 °C, <sup>1</sup>H NMR (DMSO-*d*<sub>6</sub>, 400 MHz) δ: 7.42 - 7.47 (m, 3H); 7.51 - 7.58 (m, 6H); 7.60 - 7.64 (m, 4H); 7.84 - 7.86 (m, 1H); 8.00 - 8.03 (m, 2H); 8.16 (d, *J* = 8, 1H); 9.04 (s, 1H). <sup>13</sup>C NMR (DMSO-*d*<sub>6</sub>, 100 MHz) δ: 106.38, 114.59, 119.71, 122.40, 123.27, 125.97, 126.35, 126.43, 128.17, 128.67, 129.21, 129.75, 130.07, 130.48, 131.18, 132.43, 133.66, 135.16, 138.82, 143.47, 147.53, 150.06. ESI-MS: 623.44 (C<sub>29</sub>H<sub>18</sub>BrF<sub>3</sub>N<sub>4</sub>O<sub>2</sub>S: [M+H]<sup>+</sup>). Anal. Calcd for C<sub>29</sub>H<sub>18</sub>BrF<sub>3</sub>N<sub>4</sub>O<sub>2</sub>S: C, 55.87; H, 2.91; N, 8.99; O, 5.13; S, 5.14; Found: C, 55.84; H, 2.95; N, 8.93.

#### 4.5.23 2-(1-phenyl-3-(4-(trifluoromethyl)phenyl)-1H-pyrazol-4-yl)-1-((4-(trifluoromethyl)phenyl)sulfonyl)-1H-benzo[d]imidazole (35)

Yellow powder, yield: 85%. M. p: 263 - 264 °C, <sup>1</sup>H NMR (DMSO-*d*<sub>6</sub>, 400 MHz) δ: 7.63 - 7.67 (m, 2H); 7.68 - 7.70 (m, 3H); 7.80 - 7.87 (m, 7H); 7.95 - 7.99 (m, 5H); 9.32 (s, 1H). <sup>13</sup>C NMR (DMSO-*d*<sub>6</sub>, 100 MHz) δ: 106.25, 114.54, 119.75, 125.40, 125.44, 125.47, 125.51, 125.89, 125.95, 126.41, 126.78, 128.71, 129.21, 129.35, 129.67, 130.49, 132.26, 133.62, 135.11, 138.80, 143.29, 150.10, 151.96. ESI-MS: 612.54 (C<sub>30</sub>H<sub>18</sub>F<sub>6</sub>N<sub>4</sub>O<sub>2</sub>S: [M+H]<sup>+</sup>). Anal. Calcd for C<sub>30</sub>H<sub>18</sub>F<sub>6</sub>N<sub>4</sub>O<sub>2</sub>S: C, 58.82; H, 2.96; N, 9.15; O, 5.22; S, 5.23; Found: C, 58.86; H, 2.94; N, 9.14.

## 4.6. Crystal structure determination

Crystal structures determination of compounds **20** and **24** were carried out on a Nonius CAD4 diffractometer equipped with graphite-mono chromated MoK $\alpha$  (*k* = 0.71073 Å) radiation. The structures were solved by direct methods and refined on *F*<sup>2</sup> by fullmatrix least-squares methods using SHELX-97. [47] All non-hydrogen atoms of compounds **20** and **24** were refined with anisotropic thermal parameters. All hydrogen atoms were placed in geometrically idealized positions and constrained to ride on their parent atoms.

#### **4.7. Cell proliferation assay (cell viability was assessed by MTT assay)**

A549 cells were cultured to log phase in DMEM medium supplemented with 10% fetal bovine serum. After diluting to  $2 \times 10^4$  cells/mL with the complete medium, 100  $\mu$ L of the obtained cell suspension was added to each well of 96-well microplates, and allowed to adhere for 12 h at 37 °C, 5% CO<sub>2</sub> atmosphere. Subsequently, cells were treated with compounds (**Table 3**) at increasing concentrations (0.01, 0.1, 1, 10  $\mu$ M) in the presence of 10% FBS for 24 h. Then 10  $\mu$ L MTT dye (5 mg/mL) was added to each well. After incubated at 37 °C for 4 h, the supernatants were removed gently and 150  $\mu$ L DMSO was added to every well. The plates were shaken properly to ensure complete solubilization for 5 min at room temperature. The absorbance was measured and recorded on an ELISA reader (EL $\times$ 800, BioTek, USA) at a test wavelength of 570 nm. In all the experiments three replicate wells were used for each drug concentration, and each assay was carried out at least three times.

#### **4.8. Effects on tubulin polymerization and colchicine binding to tubulin.**

27 compounds including positive control agents colchicine and CA-4 were pre-incubated at certain concentrations with 10  $\mu$ M bovine brain tubulin in glutamate buffer at 30 °C, then cooled to 0 °C. After an addition of 0.4 mM GTP, the mixtures were transferred to 0 °C cuvettes in a recording spectrophotometer and warmed to 30 °C. Tubulin polymerization was followed turbidimetrically at 350 nm. The IC<sub>50</sub> was defined as the compound concentration that inhibited the extent of polymerization by 50% after 20 min incubation.

The capacity of the test compounds to inhibit colchicine binding to tubulin was measured as described above (tubulin polymerization effect) except that the reaction mixtures contained 1  $\mu$ M tubulin, 5  $\mu$ M [<sup>3</sup>H]Colchicine, and 5  $\mu$ M test compound. Further, the binding site-specific competition examination between synthesized compounds and vinblastine was conducted as the same as colchicine.

#### **4.9. Cytotoxicity test of 293T and primary mouse hepatocyte.**

293T Cell lines and primary mouse hepatocyte were grown to log phase in DMEM supplemented with 10% fetal bovine serum, under a humidified atmosphere of 5% CO<sub>2</sub> at 37 °C. After diluting to  $1 \times 10^4$ /mL cells with the complete medium,

100  $\mu\text{L}$  of the obtained cell suspension was added to each well of 96-well culture plates and then allowed to adhere for 12 h at 37 °C, 5%  $\text{CO}_2$  atmosphere. Tested samples at pre-set concentrations (0.1, 1.0, 10, and 100  $\mu\text{M}$ ) were added to 96 wells with colchicine and CA-4 as positive drugs. For the cytotoxicity assay, 20  $\mu\text{L}$  of MTT (5 mg  $\text{mL}^{-1}$ ) was added per well 4 h before the end of the incubation. After removing the supernatant, 200  $\mu\text{L}$  DMSO was added to dissolve the formazan crystals. The absorbance at 570 nm was read on an ELISA reader (Tecan, Austria).

#### **4.10. Flow cytometry**

##### **4.10.1. Cell cycle analysis**

A549 cells were seeded in 6-well plates ( $5.0 \times 10^3$  cells/well) and incubated at 37 °C for 24 h. Exponentially growing cells were then incubated with compound **30** at different concentrations: 0, 0.1, 0.3 and 0.5  $\mu\text{M}$  for 24 h. After incubation, cells were harvested, washed with cold PBS and fixed with 70% ethanol at 4 °C overnight. The fixed cells were washed with PBS, stained with 50  $\mu\text{g}/\text{ml}$  of propidium iodide (PI) containing 100  $\mu\text{g}/\text{ml}$  of RNase A and 1% Triton X-100 in the dark for 45 min. Cellular DNA content, for cell cycle distribution analysis, was measured by flow cytometry using BD Accuri C6 Flow Cytometer (BD, USA) plotting 10000 events per sample. The percentage of cells in the G1, S and G2/M phases of the cell cycle were determined using the Flowjo 7.6 software after cell debris exclusion.

##### **4.10.2. Analysis of apoptosis**

For cell apoptosis assay, A549 cells were stained with AnnexinV-FITC and PI and then monitored for apoptosis by flow cytometry. Briefly, Approximately  $5.0 \times 10^3$  cells were seeded in 6-well plates for 24 h and then were treated with compound **30** (0, 0.1, 0.3, 0.5  $\mu\text{M}$ ) for 24 h. Then the cells were collected and washed twice with PBS and stained with 5  $\mu\text{L}$  of Annexin V-FITC and 2.5  $\mu\text{L}$  of PI (5  $\mu\text{g}/\text{mL}$ ) in 1  $\times$  binding buffer (10 mM HEPES, pH 7.4, 140 mM NaOH, 2.5 mM  $\text{CaCl}_2$ ) for 30 min at room temperature in the dark. Apoptotic cells were quantified using BD Accuri C6 Flow Cytometer (BD, USA). Statistical analysis was done using Flowjo 7.6 software.

#### **4.11. Immunofluorescence microscopy**

A549 cells were incubated in DMEM, supplemented with 10% FBS on poly

-D-lysine (Sigma-Aldrich)-coated glass coverslips in 6-well plates. Cells were seeded and allowed to adhere for at least 12 h before drugs addition. Compound **33** was diluted into 0, 0.2 and 0.5  $\mu\text{M}$ , which were added to the cells separately. After incubating for 24 h, cells were fixed by incubation in 4% paraformaldehyde for 15 min at 37 °C, then washed with PBS three times and permeabilized with 1% Triton X-100 in PBS for 10 min. After that, cells were blocked with 5% BSA for 1 h. Subsequently, these cells were washed with PBS, and incubated with anti-tubulin antibody in 3% BSA (1:200 Cytoskeleton, Inc.) at 4 °C overnight. After being washed with PBS for three times, each cover slip was added 200  $\mu\text{L}$  of Cy3-labeled goat anti-mouse IgG (H + L) in 3% BSA (1:500, Cytoskeleton, Inc.) and incubated at room temperature for 1 h. Finally, A549 cells were stained with 200  $\mu\text{L}$  of DAPI for 5 min and observed under a confocal microscope (Olympus, USA).

#### **4.12. Docking simulations**

Molecular modeling in this study was conducted by using CDOCKER protocol in Discovery Studio 3.5 (Discovery Studio 3.5, Accelrys, Inc. San Diego, CA). Crystal structures of tubulin (PDB code: 1SA0) was chosen as the template, and the pdb file was obtained from the RCSB protein data bank (<http://www.pdb.org>). The molecular docking procedure was performed by using CDOCKER protocol for receptor-ligand interactions section of Discovery Studio 3.5. [48] All bound water and ligands were eliminated from the protein and the polar hydrogen was added. The whole tubulin complex was defined as a receptor and the site sphere was selected based on the ligand binding location of colchicine (CN2700), then the CN2700 molecule was removed and one compound was placed during the molecular docking procedure.

During the molecular docking study, all 25 compounds were docked into the active site of the receptor tubulin. The CDocker Interaction Energy (interaction energy between the ligand and the receptor) agrees with the tubulin inhibitory trend. Types of interactions of the docked protein with ligand were analyzed after the end of molecular docking. In addition, 3D pose of some compounds with tubulin were also displayed using Discovery Studio 3.5 client.

**Conflicts of interest**

There are no conflicts to declare.

**Acknowledgments**

This work was supported by NSFC (31471810, 31272081), National Key R&D Program of China (SQ2017YFNC060022-05, 2017YFC0506005), and China Postdoctoral Science Foundation funded project (No. 2018M641927).

## References:

1. Nogales E, Whittaker M, Milligan RA, et al. High-resolution model of the microtubule. *Cell*. 1999;96:79-88.
2. Farce A, Loge C, Gallet S, et al. Docking study of ligands into the colchicine binding site of tubulin. *J. Enzym. Inhib. Med. Chem.* 2004;19:541-547.
3. Westermann S, Weber K. Post-translational modifications regulate microtubule function. *Nat. Rev. Mol. Cell Biol.* 2003;4:938-948.
4. Gregory RK, Smith IE. Vinorelbine-a clinical review. *Brit. J. Cancer.* 2000;82:1907.
5. Rai A, Surolia A, Panda D. An antitubulin agent BCFMT inhibits proliferation of cancer cells and induces cell death by inhibiting microtubule dynamics. *PLoS One.* 2012;7:44311.
6. Jordan A, Hadfield JA, Lawrence NJ, et al. Tubulin as a target for anticancer drugs: agents which interact with the mitotic spindle. *Med. Res. Rev.* 1998;18:259-296.
7. Kaur R, Kaur G, Gill RK et al. Recent developments in tubulin polymerization inhibitors: an overview. *Eur. J. Med. Chem.* 2014;87:89-124.
8. Liu YM, Chen HL, Lee HY, et al. Tubulin inhibitors: a patent review. *Expert Opin. Ther. Pat.* 2014;24:69-88.
9. Jordan MA, Kamath K, Manna T, et al. The primary antimetabolic mechanism of action of the synthetic halichondrin E7389 is suppression of microtubule growth. *Nat. Rev. Cancer.* 2005;4:1086-1095.
10. Sorger PK, Dobles M, Tournebise R, et al. Coupling cell division and cell death to microtubule dynamics. *Curr. Opin. Cell. Biol.* 1997;9:807-814.
11. Blagosklonny MV, Giannakakou P, Eldeiry WS, et al. Raf-1/bcl-2 phosphorylation: a step from microtubule damage to cell death. *Cancer Res.* 1997;57:130-135.
12. Lin CM, Singh SB, Chu PS, et al. Interactions of tubulin with potent natural and synthetic analogs of the antimetabolic agent combretastatin: a structural-activity study. *Mol. Pharmacol.* 1998;34:200-208.

13. Bellina F, Cauteruccio S, Monti S, et al. Novel imidazole-based combretastatin A-4 analogues: evaluation of their in vitro antitumor activity and molecular modeling study of their binding to the colchicine site of tubulin. *Bioorg. Med. Chem. Lett.* 2006;16:5757-5762.
14. Teicher BA. Newer cytotoxic agents: attacking cancer broadly. *Clin. Cancer Res.* 2008;14:1610-1617.
15. Honore S, Pasquier E, Braguer D, et al. Understanding microtubule dynamics for improved cancer therapy. *Cell. Mol. Life Sci.* 2005;62:3039-3056.
16. Garland DL. Kinetics and mechanism of colchicine binding to tubulin: evidence for ligand-induced conformational change. *Biochemistry-US.* 1978;17:4266-4272.
17. Tron GC, Pirali T, Sorba G, et al. Medicinal chemistry of Combretastatin A4: present and future directions. *Cheminform.* 2006;37:3033-3044.
18. La RG, Sarkar T, Bai R, et al. New arylthioindoles and related bioisosteres at the sulfur bridging group. 4. Synthesis, tubulin polymerization, cell growth inhibition, and molecular modeling studies. *J. Med. Chem.* 2009;52:7512-7527.
19. Nam NH. Combretastatin A-4 analogues as antimetabolic antitumor agents. *Curr. Med. Chem.* 2003;10:1697-1722.
20. Yoshino H, Ueda N, Nijima J, et al. Novel sulfonamides as potential, systemically active antitumor agents. *J. Med. Chem.* 1992;35:2496-2497.
21. Tanaka H, Ohshima N, Ikenoya M, et al. HMN-176, an active metabolite of the synthetic antitumor agent HMN-214, restores chemosensitivity to multidrug-resistant cells by targeting the transcription factor NF- $\kappa$ B. *Cancer Res.*, 2003;63:6942-6947.
22. Wang YT, Cai XC, Shi TQ, et al. Synthesis, molecular docking and biological evaluation of 1-phenylsulphonyl-2-(1-methylindol-3-yl)-benzimidazole derivatives as novel potential tubulin assembling inhibitors. *Chem. Biol. Drug Des.* 2017;90:112-118.
23. Chang JY, Lai MJ, Chang YT, et al. Synthesis and biological evaluation of 7-arylidoline-1-benzenesulfonamides as a novel class of potent anticancer agents. *Med. Chem. Comm.* 2010;1:152-155.

24. Lee HY, Pan SL, Su MC, et al. Furanylazaindoles: potent anticancer agents in vitro and in vivo. *J. Med. Chem.* 2013;56:8008-8018.
25. Xie F, Zhao H, Li D, et al. Synthesis and biological evaluation of 2,4,5-substituted pyrimidines as a new class of tubulin polymerization inhibitors. *J. Med. Chem.* 2011;54:3200-3205.
26. Marzaro G, Coluccia A, Ferrarese A, et al. Discovery of Biaryl-aminoquinazolines as novel tubulin polymerization inhibitors. *J. Med. Chem.* 2014;57:4598-4605.
27. Youn SW, Bihn JH, Kim BS. Pd-catalyzed intramolecular oxidative C-H amination: synthesis of carbazole. *Org. Lett.* 2011;13:3738-3741.
28. Rajeshkumar V, Lee TH, Chuang SC. Palladium-catalyzed oxidative insertion of carbon monoxide to N-sulfonyl-2-aminobiaryls through C-H bond activation: access to bioactive phenanthridinone derivatives in one pot. *Org. Lett.* 2013;15:1468-1471.
29. Liang Z, Zhang J, Liu Z, et al. Pd (II)-catalyzed C(sp<sup>2</sup>)-H carbonylation of biaryl-2-amine: synthesis of phenanthridinones. *Tetrahedron.* 2013;69:6519-6526.
30. Meng J, Geng R, Zhou C, et al. Advances in the research of benzimidazole drugs. *Chin. New Drugs J.* 2009;18:1505-1514.
31. Egevad L, Valdman A, Wiklund NP, et al. Beta-tubulin III expression in prostate cancer. *Scand. J. Urol. Nephrol.* 2010;44:371-377.
32. Gan LL, Shi Y, Zhou HC. Synthesis of piperazin-benzimidazole and the study of antimicrobial activity and anticancer activity, Oct. 18, Chongqing, China, pp. 113.
33. Huang J. The regulation of benzimidazole against four-stranded G-quadruplex and the study of anticancer activity and the detection of four-stranded G-quadruplex with visualization method. [D] Wuhan University, 2010.
34. Sharma S, Poliks B, Chiauzzi C, et al. Characterization of the colchicine binding site on avian tubulin isotype beta VI. *Biochemistry-US.* 2010;49:2932-2942.
35. Sierra-Fonseca JA, Bracamontes C, Saldecke J, et al. Activation of beta- and alpha-2-adrenergic receptors stimulate tubulin polymerization and promote the association of G beta gamma with microtubules in cultured NIH3T3 cells. *Biochem. Biophys. Res. Co.* 2018;1:102-108.

36. Tanitame A, Oyamada Y, Ofuji K, et al. Synthesis and antibacterial activity of a novel series of potent DNA gyrase inhibitors. Pyrazole derivatives. *Bioorg. Med. Chem.* 2004;47:3693-3696.
37. Penning TD, Talley JJ, Bertenshaw SR, et al. Synthesis and biological evaluation of the 1,5-Diarylpyrazole class of cyclooxygenase-2 inhibitors: identification of 4-[5-(4-Methylphenyl)-3-(trifluoromethyl)-1H-pyrazol-1-yl]benzenesulfonamide (SC-58635, Celecoxib). *J. Med. Chem.* 1997;40:1347-1365.
38. Bostancıoğlu RB, Demirel S, Turgut CG, et al. Novel ferrocenyl-containing N-acetyl-2-pyrazolines inhibit in vitro angiogenesis and human lung cancer growth by interfering with F-actin stress fiber polymerization. *Drug Chem. Toxicol.* 2013;36:484-495.
39. Lv J, Cao MQ, Yu JC. Alantolactone pyrazoline analogue inhibits cancer cell proliferation and induces apoptosis in non-small cell lung carcinoma cells. *Bangl. J. Pharmacol.* 2015;10:409-415.
40. Wang YT, Qin YJ, Zhang YL, et al. Synthesis, biological evaluation, and molecular docking studies of novel chalcone oxime derivatives as potential tubulin polymerization inhibitors. *RSC Adv.* 2014;4:32263-32275.
41. D'Amato RJ, Lin CM, Flynn E, et al. 2-Methoxyestradiol, an endogenous mammalian metabolite, inhibits tubulin polymerization by interacting at the colchicine site. *Proc. Natl. Acad. Sci. USA.* 1994;91:3964-3968.
42. Bonne D, Heusele C, Simon C, et al. Diamidino-2-phenylindole, a fluorescent probe for tubulin and microtubules. *J. Bio. Chem.* 1985;260:2819-2825.
43. Hou J, Lü AL; Liu BW, et al. Combination of BMP-2 and 5-AZA is advantageous in rat bone marrow-derived mesenchymal stem cells differentiation into cardiomyocytes. *Cell Bio. Int.* 2013;37:1291-1299.
44. Egan WJ, Merz KM, Baldwin JJ. Prediction of drug absorption using multivariate statistics. *J. Med. Chem.* 2000;43:3867-3877.
45. Regina GL, Bai R, Rensen WM, et al. Toward highly potent cancer agents by modulating the C-2 group of the arylthylindole class of tubulin polymerization inhibitors. *J. Med. Chem.* 2013;56:123-149.

46. Romagnoli R, Baraldi PG, Salvador MK, et al. Synthesis and evaluation of 1,5-disubstituted tetrazoles as rigid analogues of combretastatin A-4 with potent antiproliferative and antitumor activity. *J. Med. Chem.* 2012;55: 5433-5445.
47. Sheldrick GM. SHELXTL-Plus program for crystal structure solution and refinement. Gottingen, Germany: University of Gottingen, 1993.
48. Wang YT, Qin YJ, Yang N, et al. Synthesis, biological evaluation, and molecular docking studies of novel 1-benzene acyl-2-(1-methylindol-3-yl)-benzimidazole derivatives as potential tubulin polymerization inhibitors *Eur. J. Med. Chem.* 2015;99:125-137.

### Highlights

- > 25 novel benzimidazole grafted benzulfamide -containing pyrazole ring derivatives have been synthesized.
- > Their biological activities were evaluated as potential tubulin assembling inhibitors.
- > Compound **30** showed the most potent inhibitory activity against cancer cell and tubulin.
- > Crystal structure of compounds **20** and **24** were determined.